Structures Research Section

TECHNICAL MEMORANDUMS

NATIONAL ADVISORY COMMITTEE FOR AERONAUTICS

No. 749

IMPACT BUCKLING OF THIN BARS IN THE ELASTIC RANGE FOR ANY END CONDITION

By Josef Taub

Luftfahrtforschung
Vol. X, No. 2, July 6, 1933
Verlag von R. Oldenbourg, München und Berlin

Washington
July 1934

NATIONAL ADVISORY COMMITTEE FOR AERONAUTICS

TECHNICAL MEMORANDUM NO. 749

IMPACT BUCKLING OF THIN BARS IN THE ELASTIC RANGE FOR ANY END CONDITION*

By Josef Taub

SUMMARY

Following a qualitative discussion of the complicated process involved in a short-period, longitudinal force applied to an originally not quite straight bar, the actual process is substituted by an idealized process for the purpose of analytical treatment. The simplifications are: the assumption of an infinitely high rate of propagation of the elastic longitudinal waves in the bar, limitation to slender bars, disregard of material damping and of rotatory inertia, the assumption of consistently small elastic deformations, the assumption of cross-sectional dimensions constant along the bar axis, the assumption of a shock-load constant in time, and the assumption of eccentricities in one plane.

Then follow the mathematical principles for resolving the differential equation of the simplified problem, particularly the developability of arbitrary functions with steady first and second and intermittently steady third and fourth derivatives into one convergent series, according to the natural functions of the homogeneous differential equation.

The problem is resolved for one type of support corresponding to the third Eulerian loading condition (pin-ended at one end, clamped at the other). The resolution for support conditions conformable to the first and fourth Eulerian load case, may be effected in the same fashion, while substantial simplifications are afforded for the Koning-Taub analysis which treated a type of support conformably to the second Eulerian load case.

---

*"Stossartige Knickbeanspruchung schlanker Stäbe im elastischen Bereich." Luftfahrtforschung, July 6, 1933, pp. 65-85.

The premise is a course of the center line of the bar in unstressed condition such that precisely the fundamental oscillation occurs during the shock, thereby ensuring different bar forms under different shock loads. But appropriate choice of one factor makes the mutual deviation of the ordinate of the bar axis small enough so as to allow a mutual comparison of the test data for different shock loads without appreciable error. Strictly speaking, the data are applicable only to the chosen bar shapes. As to the effect of a minor change in bar shape, we refer to the appendix of the Koning-Taub report on the same subject (reference 1).

The resolution of the differential equation affords the moment formulas during the effective period of the shock load. After the actual shock, free oscillations occur whose amplitudes are given through the condition (deflection and rate) at the end of the actual shock (expansion in series, according to the natural functions of the free oscillations). An upper limit is established for the moments after the actual shock. The investigation is effected separately for shock loads smaller and greater than the Eulerian load for mathematical and physical reasons.

The results are evaluated by comparison with the moments set up by a static load equivalent to the shock load. The determination of those moments for loads greater than the Eulerian loads involves great difficulties, however, with stated eccentricities, so the interpretation of the results above the Eulerian load is effected by comparison of the data for the range of shock loads below the Euler load.

The results are as follows: The ratio of maximum moment due to shock and static load is for stated eccentricities unaffected by the magnitude of the latter. For short shock periods this ratio is less, for longer shock periods greater than 1. Its maximum generally occurs only after the actual effect of the shock load (that is, during the free oscillations) when the greatest deflection possible in this shock period is reached during the actual shock period. The maximum value further increases with increased shock loads in two (at shock load = 0) cases analyzed herein to 3.4 (at shock loads approaching the Eulerian load). The excess stresses pertaining to identical shock loads due to the shock-like stress decrease on the whole with increased shock loads. These results refer to shock loads lower than Eulerian load.

Whereas the moments in shock loads below Eulerian load attain a maximum which is not exceeded during any shock period, they increase unrestrictedly with the shock period at shock loads above Eulerian load.

In contrast with static loads, the Euler load may equally be exceeded in shock loads when the shock period is adequately short.

The results are illustrated by numerical examples and the range of validity of the approximated differential equation proved thereby.

I. INTRODUCTION

Whereas the behavior of structural components in purely static stresses is comparatively well known, the same may not be said of dynamic stresses. The probable cause is that the investigation of dynamic stresses due to appearance of an additional dimension, that is, the time factor is, a priori, more complicated than the study of conditions produced under static loads.

As a matter of fact, stress and deformation conditions of structures are always due to outside interferences which change with respect to time. Strictly speaking, their study therefore always affords a dynamic problem. On the other hand, the time rate of change of these outside interferences is, in many cases, so slow that the ensuing inner mass forces are negligibly small relative to the other (elastic or plastic) inside forces, with the result that the conditions may be accurately enough described in a simple static investigation. This is, however, no longer permissible in cases wherein the outside interactions are rapidly changing.

In bridge, and specifically in airplane design, however, the occurrence of shock-like load effects is very frequent, so that the static test supplies no longer any reliable basis for the estimation of the strength of the structural parts. While high factors of safety and the assumption of an impact factor assures the safety of bridges, even without extensive dynamic studies, this condition does not prevail in airplane design on account of the weight increase involved. The problem of the airplane designer is to ascertain the true inner and outside loads

and to fit the dimensions to the loads as closely as possible.

The present paper, an attempt in this direction, treats the hitherto neglected problem of dynamic stress, and specifically the behavior of an originally not quite straight bar in buckling under shock load. The study was prompted by a report of C. Koning on the same subject (reference 1), and which was translated into German and extended by the writer in collaboration with the DVL and the Rijks-Studiedienst voor de Luchtvaart, Amsterdam.

II. NOTATION

Q	kg,	shear.
S	kg,	tension.
$P = - X$	kg,	compression.
P_E	kg,	Eulerian buckling load.
$\underline{A}, \underline{B}$,	kg,	support reaction perpendicular to compression.
M	kgm,	bending moment.
x	m,	abscissa measured parallel to load P.
s	m,	abscissa measured parallel to bar axis.
y	m,	ordinate of bar axis in unstressed condition.
ϵ	m,	"amplitude" of bar axis in unstressed condition.
$\eta = \eta_x \eta_t$	m,	deflection $\begin{cases} \eta_x = \text{place function.} \\ \eta_t = \text{time function.} \end{cases}$
δ	m,	sag of point of application of compression P.
l	m,	bar length (chord length in approximations).
σ	m,	chord length.

ξ	m,	distance of pulsating shear from origin of coordinates.
α,		subtending slope of elastic line.
r	m,	radius of curvature of elastic line.
F	m^2,	cross-sectional area.
J	m^4,	axial moment of inertia of area.
i	m,	inertial radius.
E	kgm^{-2},	modulus of elasticity.
G	kgm^{-2},	shear modulus.
ρ	$kgs^2\ m^{-4}$,	density.
t	s,	time coordinate.
τ	s,	shock period.
$\bar{t} = t-\tau$	s,	time coordinate.
T	s,	period of free transverse fundamental oscillation.
p	s^{-1},	frequency.
φ,		phase shifting.
$\lambda, \bar{\lambda}$	m^{-1},	proper values.
$K(x, \xi)$,		core functions.
a,		see equation (35).
$a_E = \frac{P}{P_E}$,		ratio of compression to Eulerian buckling load, i.e., the reciprocal value of the static buckling strength.
$b = \frac{\tau}{T}$,		ratio of shock period to oscillation period of the free transverse fundamental oscillation.
c,		ratio of absolute maximum moment in the static and dynamic case.

μ, constant value (compare equation (31)).

A_n, nth coefficient of a series expansion.

$A, B, C, D, \bar{A}, \bar{B}, c_1, c_2, k_1, k_2$, integration constants.

Indices:

$m, n = 1, 2, 3 \ldots$ the natural figures.

0 refers to quantities occurring with tension $P = 0$.

E, quantities occurring with Eulerian buckling load.

l, r denote quantities to the left or right of ξ.

x, place function.

t, time function.

Signs of differences:

η_x', η_x'', η_x''', η_x'''' denote the 1st, 2d, 3d, 4th derivative of η_x, according to x.

$\dot{\eta}_t$, $\ddot{\eta}_t$ denote 1st, 2d derivative of η_t, according to t.

III. QUALITATIVE DISCUSSION OF PROCESS

The qualitative description of the buckling stress due to shock load is as follows:

An arbitrarily supported, originally unstressed, elastic bar is suddenly subjected to a longitudinal force constant or variable with respect to time. If the bar axis is straight and the load is coincident with it, a so-called "dilatation wave" is produced in the bar, i.e., a longitudinal wave consisting of compressions or thinnings (or groups of such waves) which, as known, travel at sonic ve-

locity $\sqrt{E/\rho}$ in the material of the bar. Arrived at the other end, the shock wave is at least partially reflected on account of the there existing discontinuities in density and elasticity. If the end is clamped fast, or consists of a free end dipped in a medium of zero density, the reflection is complete. In the further course the original (primary) waves superpose themselves onto the reflected (secondary) waves. When the excitation of the shock waves is harmonic and in absence of material damping (i.e., zero viscosity of material) the superposition of the primary and completely reflected secondary waves produces so-called standing waves, that is, waves with fixed nodes. But allowing for material damping and energy scatter at the points of discontinuity, there still remain apart from the standing waves which are of lower amplitude in this case than before, the so-called "advancing waves." A detailed report on this phenomenon - although limited to transverse waves - has been published by Katsutade Sezawa (reference 2).

In unharmonic shock excitations the type of superposition depends on the type of excitation. The case, for example, of a bar hit by a certain mass at a certain rate, and of a bar struck by a mass of zero velocity ("suddenly loaded bar") with disregard as to viscosity and presumed maintenance of energy (i.e., absence of energy scatter at the points of discontinuity of density and elasticity) has been treated by several authors (reference 3). Once the first disturbance, moving at the rate of $\sqrt{E/\rho}$ has covered the length of the bar, the latter is in a variable stress condition throughout its length both with respect to time and place.

After the shock, that is, after the contact between the shock mass and the bar has ceased, the bar evinces wave motions corresponding to the free oscillation forms. The initial conditions of this period of motion are contingent upon the condition existent at the end of the actual shock. The stress condition of the bar is equally variable in time and place in the period after the shock.

Now, if the bar axis is not exactly straight or if the shock load is eccentric, the results are bending waves in addition to the longitudinal waves. The rate of motion of these waves is, however, contrary to that of the longitudinal waves, dependent upon the wave length. Unless the frequency is unduly high, it is inversely proportional to

the wave lengths; at high frequencies and when the waves consist of various groups, other laws are applicable. With vanishing wave length the rate of motion approaches that of the Rayleigh waves ($v = 0.9194\sqrt{\frac{G}{\rho}}$, reference 4). The rate of movement of the bending waves is also considerably lower than that of the longitudinal waves. As to reflection and superposition of bending waves at points of discontinuities, the same laws apply as to the longitudinal waves.

By virtue of the fact that the longitudinal waves move faster than the bending waves, the point of origin of the latter is not only limited to the shocked bar end in the case of the bar hit by a longitudinal force, as is the case for the longitudinal wave. Rather a bending wave comes into being successively at every point of the bar, as soon as the longitudinal wave has reached the particular point. Each one of these bending waves spreads to the right and left of its point of origin to be reflected at the points of discontinuity of density and elasticity and to superpose themselves upon each other. But the rate of movement of these bending waves is in this case unlike the usual bending waves, since they move in a more or less compressed part of the bar rather than in an unstressed bar. According to Sezawa (reference 2), the rate of motion of the bending waves decreases as the compression in the bar increases. For buckling stress due to shock, the difference in rate of movement of the longitudinal and the transverse waves will therefore be even greater than otherwise.

According to this qualitative discourse, the processes in shock loads in buckling are very complicated, and to follow them mathematically requires various simplifying assumptions.

IV. SIMPLIFYING ASSUMPTIONS

1. The first assumption is infinitely great rate of movement of the longitudinal waves, or in other words, that the bar reaches longitudinal stress condition within infinitely short time. Then the bending waves emanating from the different points of the bar are simultaneously excited rather than successively, and instead of a wave motion there are standing oscillations to begin with.

This assumption is the more applicable as the frequency of the shock motion is lower and the shock force greater, because both factors tend to lower the rate of movement of the bending waves but not that of the longitudinal waves. Moreover, it is anticipated that the conditions of the oscillating bar corresponding to this assumption will more closely approach actual conditions as the time interval between entry of disturbance, i.e., start of shock and end of shock is greater.

On these premises the analysis is restricted to the effect of the bending oscillations. The stress due to the longitudinal force is readily obtained by dividing the momentary shock load by the cross-sectional area.

2. The study is confined to the investigation of buckling due to shock in slender bars. From the cited qualitative analysis it follows that the energy of the shock mass goes partly into bending and partly into longitudinal oscillation energy of the bar. The component of the bending oscillation increases with the slenderness of the bar as seen hereinafter.

A bar pin-ended at both sides (fig. 1a) is subjected to static compression P. Presumedly, the bar was not quite straight at the start and the deviation of its axis from a straight line corresponds to a half sine wave. It can be proved that the elastic line is sinusoidal in this case also. With the arc length as independent variable (reference 5), we have:

$$y = \epsilon \sin \frac{\pi}{l} s \tag{1}$$

$$\eta = \eta_{max} \sin \frac{\pi}{l} s \tag{2}$$

Moreover, according to figure 1b:

$$\frac{d(\eta + y)}{ds} = \sin \alpha \tag{3}$$

The chord length follows from

$$\sigma = \int dx = \int_0^l \cos \alpha \, ds \tag{4}$$

In second approach $\cos \alpha$ may be replaced by (reference 5):

$$\cos \alpha = 1 - \frac{\alpha^2}{2} = 1 - \frac{\sin^2 \alpha}{2}$$

or, because of (3), by

$$\cos \alpha = 1 - \frac{1}{2} \left[\frac{d(\eta + y)}{ds}\right]^2 .$$

This value of $\cos \alpha$ written in (4) gives with due allowance for (1) and (2):

$$\sigma = \int_0^l \left[1 - \frac{1}{2} (\epsilon^2 + 2 \epsilon \eta_{max} + \eta_{max}^2) \frac{\pi^2}{l^2} \cos^2 \frac{\pi}{l} s\right] ds =$$

$$= l - \frac{\pi^2}{4l} (\epsilon^2 + 2 \epsilon \eta_{max} + \eta_{max}^2).$$

By the same argument the chord length prior to loading is:

$$\sigma_o = l - \frac{\pi^2}{4l} \epsilon^2$$

Consequently, the sag of the applied moment of the load is:

$$\delta = \sigma_o - \sigma = \frac{\pi^2}{4l} (\eta_{max}^2 + 2 \epsilon \eta_{max}) \qquad (5)$$

The deflection in bar center in this case is conformable to the Koning-Taub report (reference 1):

$$\eta_{max} = \frac{\epsilon}{\frac{P_E}{P} - 1} \qquad (6)$$

with $P_E = \frac{\pi^2 E J}{l^2}$ the Eulerian buckling load.

With $a = \frac{P}{P_E}$, (5) and (6) give:

$$\delta = \frac{\pi^2 \epsilon^2}{4 l} \frac{a(2 - a)}{(1 - a)^2} \qquad (7)$$

This formula yields δ/ϵ^2 versus l, whereby it is to be remembered that l implicitly occurs also in P_E. The curves obtained for stated P, E, and J values are on the order of those shown in figure 2. As the slenderness of the bar increases the displacement δ of the applied

moment increases much more rapidly than linear even when ϵ is assumed as being constant. On top of that ϵ, that is, the probable maximum deviation of the bar from straight, is frequently assumed so much greater as the bar is thinner. (Müller-Breslau, for instance, figures with an initial eccentricity of $l/200$.)

Thus, while the sag of the point of applied moment increases with the length of the bar at a much faster rate than linear, that due to the longitudinal compression increases only linearly with the bar length (Hooke's law). Therefore, the more slender the bar, the greater the deflection compared to the displacement of the applied moment of the force due to compression. Assuming for simplicity that the force P is constant in time, the energy required to deflect or compress the bar is simply proportional to the deflection or compression or, in other words, the ratio of both is actually so much higher as the bar is more slender.

Hence the omission of the longitudinal oscillations appear still more justified since the investigation is confined to slender bars.

3. The damping effect due to material viscosity is also ignored as its effect will be rather negligible in the short period processes involved here, although its inclusion should cause no insuperable difficulties.

4. All investigations retain their validity only in stresses below the elastic limit.

5. The deviations from straight line as well as the deflections are assumed to be small quantities compared to the length of the bar, so that the curvature of the elastic line may be accurately enough defined with $d^2\eta/dx^2$. The scope of validity of this assumption is analyzed in a subsequent section.

6. We assume a bar with sectional area constant along the bar axis, with constant inertia moment and elasticity modulus.

7. The transverse (bending) oscillations are treated as plane problem, i.e., all deviations from straight line are presumed to lie in one plane.

8. As to the time rate of shock, it is simply assumed that the shock load is a constant independent of time. Although this may not exactly correspond to the actual shock of landing of an airplane or other similar shock loads, it is a good approach in the majority of cases.

9. The effect of the rotatory inertia is disregarded, i.e., the term $\rho J \frac{\partial^4 \eta}{\partial t^2 \partial x^2}$ is deleted in the differential equation.

V. DIFFERENTIAL EQUATIONS AND BASIS OF RESOLUTION

1. Generalities

The approximate differential equation is

$$E J \frac{\partial^4 \eta}{\partial x^4} - X \frac{\partial^2 \eta}{\partial x^2} + \rho F \frac{\partial^2 \eta}{\partial t^2} = X \frac{\partial^2 y}{\partial x^2} \qquad (8)$$

(X must be written with positive sign as tension.) The resolution of this equation, i.e., the determination of the transverse oscillations of a bar loaded under constant tension X, whose center line in unstressed condition is $y = f(x)$, is readily tractable for the case of a bar hinged at both ends, by expanding $y = f(x)$ in a series whose individual terms correspond to the natural functions of the free bar oscillation.

For the generalized case (i.e., any support condition) the expansion of $f(x)$ conformably to the natural functions of the free bar oscillation is abortive. It rather necessitates the development of the right-hand side of (8) according to the natural functions of the homogeneous equation

$$E J \frac{\partial^4 \eta}{\partial x^4} - X \frac{\partial^2 \eta}{\partial x^2} + \rho F \frac{\partial^2 \eta}{\partial t^2} = 0 \qquad (9)$$

the differential equation of the straight bar stressed in tension X. It possesses mutually orthogonal natural functions, from which arbitrary functions may be developed in convergent series.

The exact proof of this developability follows from a

Hilbert theorem (reference 6), conformable to which any function (reference 7), according to the natural functions of a continuous symmetrical core may be expanded in a convergent series.

The source-like representation of the elastic line is obtained with the so-called "influence function" (Green function). This is the equation of the elastic line with x as independent variable due to a force 1 acting at point $x = \xi$. According to whether $x \leqq \xi$ or $x \geqq \xi$, the results are two different terms, which are denoted by $K_l(x, \xi)$ and $K_r(x, \xi)$, respectively. Maxwell's law of mutual displacements states that a force 1 acting at point ξ causes the same deflection at x as a force 1 acting at x in ξ. Therefore, the influence functions $K_l(x, \xi)$ valid for $x \leqq \xi$ and $K_r(x, \xi)$ valid for $x \geqq \xi$ are symmetrical - (the appendix gives as examples the symmetrical influence functions for the support conditions corresponding to the second and third Euler case) - that is,

$$K_l(x, \xi) = K_r(\xi, x).$$

But this influence function is exactly the core function of the integral equation, thus proving the developability according to natural functions.

Maxwell's law adduced as proof of the validity to a bar compressed in constant tension and bent in arbitrary shear follows from the fact that the premise of Maxwell's law: the law of linear superposition is equally valid, provided the tension remains unaltered. The validity of the law of superposition follows from the linearity of the differential equation (9), which is briefly discussed in the next two sections with particular reference to the corresponding natural functions and period equations for the support conditions characterizing the four Eulerian cases.

2. Transverse Oscillations of a Straight Bar Loaded in Tension

a) Solution of the homogeneous differential equation.- The particular solutions of synchronous character of (9) in conformity with the first assumption, are:

$$\eta = \eta_t \, \eta_x$$

with $\eta_t = f(t)$ and $\eta_x = f(x)$. Putting

$$\eta = \sin p t \, e^{\kappa x}$$

in (9), yields the typical equation:

$$E J \kappa^4 - X \kappa^2 - \rho F p^2 = 0 \qquad (10)$$

of the four roots,

$$\kappa = \pm \sqrt{\frac{X}{2EJ} \pm \sqrt{\frac{X^2}{4 E^2 J^2} + \frac{\rho F}{EJ} p^2}} \qquad (11)$$

of (10): $\kappa_1 = \pm \lambda$ are real for real values of p, and two, $\kappa_2 = \pm \lambda i$ are imaginary, and this holds for positive X (tension) as well as negative X (compression). Then the solution reads:

$$\eta_x = A \operatorname{ch} \lambda x + B \operatorname{sh} \lambda x + C \cos \bar{\lambda} x + D \sin \bar{\lambda} x \qquad (12)$$

For imaginary values of p, we obtain four real roots, $\kappa_1 = \pm \lambda i$ and $\kappa_2 = \pm \bar{\lambda} i$ with positive X when assuming that

$$\frac{X^2}{4 E^2 J^2} > \left| \frac{\rho F}{EJ} p^2 \right| \qquad (13)$$

For tension loads (12) then becomes

$$\eta_x = A \operatorname{ch} \lambda x + B \operatorname{sh} \lambda x + C \operatorname{ch} \bar{\lambda} x + D \operatorname{sh} \bar{\lambda} x \qquad (14)$$

and for compressive loads,

$$\eta_x = A \cos \lambda x + B \sin \lambda x + C \cos \bar{\lambda} x + D \sin \bar{\lambda} x \qquad (15)$$

Imaginary values of p occur according to VI,3,b in compression exceeding the Eulerian load. The same section also discloses that (13) is met so long as the compression is not in excess of twice the Eulerian load. Compressive stresses beyond this double Eulerian load are without the scope of this report.

It also follows from (11) that

$$\kappa_1^2 + \kappa_2^2 = \lambda^2 - \bar{\lambda}^2 = \frac{X}{EJ} \qquad (16)$$

whereby (9) becomes

$$[(E J \lambda^2 - X) \lambda^2 \eta_t + \rho F \ddot{\eta}_t] \eta_x = 0 \qquad (17)$$

From (16) follows $\bar{\lambda} = \lambda$ when $X = 0$. Without tension the term for η_x thus becomes

$$\eta_x = A \operatorname{ch} \lambda x + B \operatorname{sh} \lambda x + C \cos \lambda x + D \sin \lambda x \qquad (18)$$

and (17) reduces to

$$(E J \lambda^4 \eta_t + \rho F \ddot{\eta}_t) \eta_x = 0 \qquad (19)$$

b) Determination of constants and derivation of the period equation for various support conditions.- In the following the constants in (12) together with the natural values of λ and $\bar{\lambda}$ are analyzed for the support conditions of the four Euler cases.

1. Euler case: one end fixed, the other free.

Boundary conditions: $\eta_x = 0$ and $\eta_x' = 0$ for $x = 0$

$\eta_x'' = 0$ for $x = l$.

The fourth is obtained for $x = l$ as follows:

For $x = l$

$$\eta_x' = \tan \alpha \sim \sin \alpha \sim \alpha,$$

hence the shear,

$$Q = - X \sin \alpha = - X \eta_x'.$$

On the other hand,

$$Q = - E J \eta_x'''$$

thus

$$\eta_x''' - \frac{X}{EJ} \eta_x' = 0 \qquad (20)$$

when $x = l$.

From the boundary conditions for $x = 0$ follows:

$A + C = 0$, consequently $C = - A$

$\lambda B + \bar{\lambda} D = 0$, " $D = - \frac{\lambda}{\bar{\lambda}} B$.

Therefore,

$$\eta_x = A(\operatorname{ch}\lambda x - \cos\bar{\lambda}x) + B(\operatorname{sh}\lambda x - \frac{\lambda}{\bar{\lambda}}\sin\bar{\lambda}x) \qquad (21)$$

With $x = l$, the boundary conditions give:

$$\eta_x'' = A(\lambda^2 \operatorname{ch}\lambda l + \bar{\lambda}^2 \cos\bar{\lambda}l) + B(\lambda^2 \operatorname{sh}\lambda l + \lambda\bar{\lambda}\sin\bar{\lambda}l) = 0 \qquad (22)$$

and

$$A(\lambda^3 \operatorname{sh}\lambda l - \bar{\lambda}^3 \sin\bar{\lambda}l) + B(\lambda^3 \operatorname{ch}\lambda l + \lambda\bar{\lambda}\cos\bar{\lambda}l) -$$

$$- \frac{X}{EJ}[A(\lambda \operatorname{sh}\lambda l + \bar{\lambda}\sin\bar{\lambda}l)] + B(\lambda \operatorname{ch}\lambda l - \lambda\cos\bar{\lambda}l) = 0$$

or, with allowance for (16)

$$A(\lambda\bar{\lambda}^2 \operatorname{sh}\lambda l - \bar{\lambda}\lambda^2 \sin\bar{\lambda}l) + B(\lambda\bar{\lambda}^2 \operatorname{ch}\lambda l + \bar{\lambda}^3 \cos\bar{\lambda}l) = 0 \qquad (23)$$

So that A and B do not disappear, the denominator determinant of (22) and (23) must be zero:

$$\begin{vmatrix} \lambda^2 \operatorname{ch}\bar{\lambda}l + \bar{\lambda}^2 \cos\bar{\lambda}l & \lambda^2 \operatorname{sh}\lambda l + \lambda\bar{\lambda}\sin\bar{\lambda}l \\ \lambda\bar{\lambda}^2 \operatorname{sh}\lambda l - \bar{\lambda}\lambda^2 \sin\bar{\lambda}l & \lambda\bar{\lambda}^2 \operatorname{ch}\lambda l + \lambda^3 \cos\bar{\lambda}l \end{vmatrix} = 0.$$

The evaluation of this determinant gives the transcendent period equation:

$$2\lambda^2\bar{\lambda}^2 + (\bar{\lambda}^4 + \lambda^4)\operatorname{ch}\lambda l \cos\bar{\lambda}l + \lambda\bar{\lambda}(\lambda^2 - \bar{\lambda}^2)\operatorname{sh}\lambda l \sin\bar{\lambda}l = 0 \qquad (24)$$

which, together with (16) gives the natural values of λ and $\bar{\lambda}$ for the different longitudinal forces.

For $X = 0$, $\bar{\lambda} = \lambda$ and (24) becomes

$$\operatorname{ch}\lambda l \cos\bar{\lambda}l + 1 = 0.$$

2. Euler case: both ends hinged.

Boundary conditions: $\eta_x = 0$ and $\eta_x'' = 0$ for $x = 0$

$\eta_x = 0$ and $\eta_x'' = 0$ for $x = l$

For $x = 0$, we have:

$$\left.\begin{aligned} A + C &= 0 \\ \lambda^2 A - \bar{\lambda}^2 C &= 0 \end{aligned}\right\} \text{ hence, } A = C = 0;$$

for $x = l$, we have:

$$\eta_x = B \operatorname{sh} \lambda l + D \sin \bar{\lambda} l = 0 \tag{25}$$

$$\eta_x'' = \lambda^2 B \operatorname{sh} \lambda l - \bar{\lambda}^2 D \sin \bar{\lambda} l = 0 \tag{26}$$

The condition, according to which the denominator determinant of these equations must disappear, gives the period equation:

$$\operatorname{sh} \lambda l \sin \bar{\lambda} l = 0.$$

This equation is fulfilled for $\sin \bar{\lambda} l = 0$, that is, for

$$\bar{\lambda} = \frac{\pi}{l}, \frac{2\pi}{l}, \ldots . \frac{n\pi}{l}.$$

From (25) and (26) further follows $B = 0$, whence the validity of

$$\eta_x = D \sin \bar{\lambda} x \tag{27}$$

Since this equation contains only $\bar{\lambda}$, the proper functions in the second Euler case are unaffected by the longitudinal force. Solution (27) is equally valid when no tension exists. For this reason it was possible in the second Euler case treated in the Koning-Taub report (reference 1) to expand the right-hand side of (8) conformably to the natural functions of the free transverse oscillations.

3. Euler case: one end clamped, the other pin-ended.

Boundary conditions: $\eta_x=0$ and $\eta_x'=0$ for $x=0$

$\eta_x=0$ and $\eta_x''=0$ for $x=l$

The conditions for $x = 0$ are the same as for the first Euler case, hence (21) is valid.

For $x = l$, we have:

$$\eta_{x=l} = A(\operatorname{ch} \lambda l - \cos \bar{\lambda} l) + B\left(\operatorname{sh} \lambda l - \frac{\lambda}{\bar{\lambda}} \sin \bar{\lambda} l\right) = 0 \tag{28}$$

$$\eta''_{x=l} = A(\lambda^2 \operatorname{ch} \lambda l + \bar{\lambda}^2 \cos \bar{\lambda} l) + B(\lambda^2 \operatorname{sh} \lambda l + \lambda \bar{\lambda} \sin \bar{\lambda} l) = 0 \tag{29}$$

The condition of vanishing denominator determinant affords:

$$(\operatorname{ch} \lambda l - \cos \bar{\lambda} l)\ (\lambda^2 \operatorname{sh} \lambda l + \lambda\bar{\lambda} \sin \bar{\lambda} l) -$$

$$- \left(\operatorname{sh} \lambda l - \frac{\lambda}{\bar{\lambda}} \sin \bar{\lambda} l\right)\ (\lambda^2 \operatorname{ch} \lambda l + \bar{\lambda}^2 \cos \bar{\lambda} l) = 0$$

and, after appropriate conversions, the transcendent period equation:

$$\frac{\lambda}{\bar{\lambda}} \tan \bar{\lambda} l - \operatorname{th} \lambda l = 0 \tag{30}$$

The roots of (30) give the natural values λ and $\bar{\lambda}$ for the different X values.

With $\mu = \frac{B}{A}$, (28) yields:

$$\mu = - \frac{\operatorname{ch} \lambda l - \cos \bar{\lambda} l}{\operatorname{sh} \lambda l - \frac{\lambda}{\bar{\lambda}} \sin \bar{\lambda} l} \tag{31}$$

which, in conjunction with (28) and (29) gives:

$$\operatorname{ch} \lambda l + \operatorname{sh} \lambda l = 0 \tag{32}$$

$$\cos \bar{\lambda} l + \mu \frac{\lambda}{\bar{\lambda}} \sin \bar{\lambda} l = 0 \tag{33}$$

For vanishing longitudinal force (X = 0) (30) becomes:

$$\tan \lambda l - \operatorname{th} \lambda l = 0 \tag{34}$$

since $\bar{\lambda} = \lambda$.

Since this paper treats the third Euler case as an example of the generalized method, the determination of the natural values requires a more detailed discussion:

The introduction of

$$a = - \frac{X}{E J \bar{\lambda}^2} \tag{35}$$

changes (16) to

$$\lambda^2 = \bar{\lambda}^2 (1 - a) \tag{36}$$

and (30) to

$$\tan \bar{\lambda} l - \frac{1}{\sqrt{1 - a}} \operatorname{th} (\bar{\lambda} l \sqrt{1 - a}) = 0 \qquad (37)$$

the roots $\bar{\lambda} l$ of this equation are obtained as intersections of the curves

$$f (\bar{\lambda}) = \tan \bar{\lambda} l$$

and

$$\bar{f} (a, \bar{\lambda}) = \frac{1}{\sqrt{1 - a}} \operatorname{th} (\bar{\lambda} l \sqrt{1 - a}) \qquad (38)$$

For $a = 1$, $\bar{f} (a, \bar{\lambda}) = \frac{0}{0}$, consequently,

$$\bar{f} (a, \bar{\lambda})_{a=1} = \frac{\frac{d}{da} [\operatorname{th} (\bar{\lambda} l \sqrt{1 - a})]}{\frac{d}{da} \sqrt{1 - a}} = \bar{\lambda} l$$

is a straight line.

For $a > 1$ (38) becomes:

$$\bar{f} (a, \bar{\lambda}) = \frac{\tan (\bar{\lambda} l \sqrt{a - 1})}{\sqrt{a - 1}}$$

Figure 3 shows the functions $f(\bar{\lambda})$ and $\bar{f}(a, \bar{\lambda})$ plotted against $\bar{\lambda} l$ for several a values (parameter).

For $a = 0$,

$$\lambda_o l = \frac{5}{4} \pi, \frac{9}{4} \pi, \ldots, \frac{4n + 1}{4} \pi, \ldots$$

is accurate enough.

All these values are at least within 0.1 percent accuracy of

$$\mu_o = - 1$$

so that,

$$\eta_{xo} = A(\operatorname{ch} \lambda_o x - \cos \lambda_o x - \operatorname{sh} \lambda_o x + \sin \lambda_o x) \qquad (39)$$

is also sufficiently exact.

In figure 4 the $\bar{\lambda}l$ values for the fundamental and the first higher oscillation have been plotted against a. Up to about $a = 1$ the $\bar{\lambda}l$ values show a slow increase with a; beginning at $a > 1$ the mean rise is steeper and the curves coil about a mean curve (dashes) which, expressed in formula, is

$$\bar{\lambda}l = \frac{n\pi}{1 - \sqrt{a - 1}} \tag{40}$$

where $n = 1$ = fundamental oscillation, and $n = 2$ = first higher oscillation. Equation (40) is exact for whole multiples of $\pi/2$. For $a = 2$, $\bar{\lambda}l = \infty$.

4. Euler case: both ends clamped.

Boundary conditions: $\eta_x=0$ and $\eta_x'=0$ for $x=0$

$\eta_x=0$ and $\eta_x'=0$ for $x=l$.

The conditions for $x = 0$ are, as in the first Euler case, so that (21) is applicable.

For $x = l$, we have:

$$\eta_{x=l} = A(\operatorname{ch} \lambda l - \cos \bar{\lambda} l) + B\left(\operatorname{sh} \lambda l - \frac{\lambda}{\bar{\lambda}} \sin \bar{\lambda} l\right) = 0$$

$$\eta'_{x=l} = A(\lambda \operatorname{sh} \lambda l + \bar{\lambda} \sin \bar{\lambda} l) + B(\lambda \operatorname{ch} \lambda l - \lambda \cos \bar{\lambda} l) = 0$$

The disappearance of the denominator determinant stipulates:

$$\lambda(\operatorname{ch} \lambda l - \cos \bar{\lambda} l)^2 - \left(\operatorname{sh} \lambda l - \frac{\lambda}{\bar{\lambda}} \sin \bar{\lambda} l\right)(\lambda \operatorname{sh} \lambda l + \bar{\lambda} \sin \bar{\lambda} l) = 0.$$

Thus the period equation is:

$$2(1 - \operatorname{ch} \lambda l \cos \bar{\lambda} l) + \frac{\lambda^2 - \bar{\lambda}^2}{\lambda \bar{\lambda}} \operatorname{sh} \lambda l \sin \bar{\lambda} l = 0 \tag{41}$$

The λ and $\bar{\lambda}$ values are obtained as roots of (16) and (41).

For $x = 0$, $\bar{\lambda} = \lambda$, so that the period equation becomes:

$$\operatorname{ch} \lambda l \cos \bar{\lambda} l = 1.$$

VI. SOLUTION OF THE UNHOMOGENEOUS DIFFERENTIAL EQUATION

1. Generalities

With the proper functions derived in V,2, we proceed in the general case by developing for given original bar form $y(x)$ the right side of (8) according to the proper functions of (9) and then pose a corresponding equation for the place function η_x in the solution $\eta = \eta_t \eta_x$ conformable to the natural functions of (9).

In view of the comparatively complex form of the natural functions together with the tedious series development of $X \frac{\partial^2 y}{\partial x^2}$, this method would, however, become quite troublesome. Added to this is the fact that different functions would have to be set up for the original bar form y, even if intending to allow for the probable cases only. It must therefore be understood that the investigation - exactly like similar ststic studies - is feasible only for stated bar forms and that the conditions anticipated for other forms must be arrived at by deduction from the obtained results.

Under these circumstances the thought lies close to discuss the general method with such a bar form as to lead to mathematically convenient formulas. The most elementary case is a bar form developing only the fundamental oscillation during the shock period. But, excepting the second Euler case, the natural values and through them the form of the fundamental oscillation differs for different X (see V,2,b - figs. 3 and 4). Accordingly, different bar forms are necessary for different X, to insure the appearance of the fundamental oscillation only. On the other hand, an analysis which presumes variable original bar forms as X increases, would be unsatisfactory as it would, to be sure, afford a comparison of the bar under a stated static load with an equivalent dynamic load, while, however, affording no possible means of comparing the processes occurring under different longitudinal forces.

However, we shall use this method for the third Euler case,* which is being analyzed to explain the general meth-

*The period equation of the third Euler case is much more simple than than that of the first and fourth Euler case (see (24), (30), and (41),) thus making the mathematical treatment of the third case somewhat more convenient than the first and third case.

od. It is possible to show that with appropriate handling of a constant the bar forms at which precisely the fundamental oscillation occurs are so little unlike under different longitudinal forces as to make comparison of the results obtained for different longitudinal forces possible without great errors.

As concerns the effect of slight modifications in the bar form, we refer to the appendix of the report cited in reference 1.

2. Choice of Interference Function (Bar Shape)

To insure that the "curved" bar executes the fundamental oscillation of the straight bar the second derivative of its original form must be chosen conformably to the first natural function of the straight bar.

Accordingly, we choose for $\frac{\partial^2 y}{\partial x^2}$

$$\frac{\partial^2 y}{\partial x^2} = - \epsilon_1 \bar{\lambda}_1^2 \left[\operatorname{ch} \lambda_1 x - \cos \bar{\lambda}_1 x + \mu \left(\operatorname{sh} \lambda_1 x - \frac{\lambda_1}{\bar{\lambda}_1} \sin \bar{\lambda}_1 x \right) \right] \tag{42}$$

which up to constant ϵ_1, agrees with the first natural function of (9). (Compare (21) and (31).)

Then (8) resolves to

$$\eta = \eta_t \quad \eta_x = \eta_t \left[\operatorname{ch} \lambda_1 x - \cos \bar{\lambda}_1 x + \mu \left(\operatorname{sh} \lambda_1 x - \frac{\lambda_1}{\bar{\lambda}_1} \sin \bar{\lambda}_1 x \right) \right] \tag{43}$$

Writing (42) and (43) in (8) and omitting the index 1, we have:

$$\left[(EJ \lambda^2 - X) \lambda^2 \eta_t + \rho F \ddot{\eta}_t + X \epsilon \bar{\lambda}^2 \right] (\operatorname{ch} \lambda x + \mu \operatorname{sh} \lambda x) -$$

$$- \left[(EJ \bar{\lambda}^2 + X) \bar{\lambda}^2 \eta_t + \rho F \ddot{\eta}_t + X \epsilon \bar{\lambda}^2 \right] (\cos \bar{\lambda} x + \mu \frac{\lambda}{\bar{\lambda}} \sin \bar{\lambda} x) = 0,$$

or, because of (16),

$$\left[(E J \bar{\lambda}^2 + X) \bar{\lambda}^2 \eta_t + \rho F \ddot{\eta}_t + X \epsilon \bar{\lambda}^2 \right] \eta_x = 0 \tag{44}$$

Now we try to ascertain to which original bar form the chosen function (42) corresponds, i.e., find the trend of the eccentricities y to ensure that the shock load X exactly produces the fundamental oscillation.

Twice integrating (42) gives:

$$y = -\epsilon\left[\frac{\bar{\lambda}^2}{\lambda^2}\operatorname{ch}\lambda x + \cos\bar{\lambda}x + \mu\left(\frac{\bar{\lambda}^2}{\lambda^2}\operatorname{sh}\lambda x + \frac{\lambda}{\bar{\lambda}}\sin\bar{\lambda}x\right)\right] + c_1 x + c_2 \quad (45)$$

Now we can prescribe certain conditions for defining c_1 and c_2. The nearest one would be to require that the boundary conditions for function y agree with those of the elastic line of the stressed bar.

The conditions then would be:

1. For $x = 0$ $\quad y = 0$
2. " $x = 0$ $\quad \frac{dy}{dx} = 0$
3. " $x = l$ $\quad y = 0$
4. " $x = l$ $\quad \frac{d^2y}{dx^2} = 0$

With only two constants available, however, only two of these conditions can be met. There are $(4/2) = 6$ possibilities.

We select that for which conditions 1 and 2 are fulfilled. It is simpler in many respects than other forms. Subsequently, it is shown that for it the maximum moment nearly always occurs at the point of fixity. Added to that is the ready comparison to bar forms under different longitudinal loads cited in VI,1. For this bar form, it is

$$c_1 = \epsilon\mu\left(\frac{\bar{\lambda}^2}{\lambda} + \lambda\right)$$

and

$$c_2 = \epsilon\left(\frac{\bar{\lambda}^2}{\lambda^2} + 1\right)$$

consequently,

$$y = -\epsilon\left[\frac{\bar{\lambda}^2}{\lambda^2}\operatorname{ch}\lambda x + \cos\bar{\lambda}x + \mu\left(\frac{\bar{\lambda}^2}{\lambda^2}\operatorname{sh}\lambda x + \frac{\lambda}{\bar{\lambda}}\sin\bar{\lambda}x\right) - \left(\frac{\bar{\lambda}^2}{\lambda^2} + 1\right)(1 + \mu\lambda x)\right] \quad (46)$$

The evaluation of (46) gives the curves shown in figure 5. The values $-\frac{y}{\epsilon}$ for $x = 0.5\,l$, $x = 0.75\,l$ and $x = l$ proportional to the ordinates of the bar form are plotted versus a. The ordinates for $x = 0.25\,l$ are too small to be representable at the scale used in figure 5.

For $a = 1$, which corresponds to the Euler load as tension, as shown elsewhere, $\lambda = 0$ because of (36), and $\mu = \frac{0}{0}$ because of (31). Thus (46) may be expressed as

$$y = -\epsilon \left[\frac{\bar{\lambda}^2}{\lambda^2}(\operatorname{ch}\lambda x - 1) + (\cos\bar{\lambda}x - 1) + \frac{\bar{\lambda}^2}{\lambda^2}\mu(\operatorname{sh}\lambda x - \lambda x) + \right.$$
$$\left. + \frac{\lambda}{\bar{\lambda}}\mu(\sin\bar{\lambda}x - \bar{\lambda}x)\right]$$

after which we determine separately the unknown terms,

$$\left[\frac{\bar{\lambda}^2}{\lambda^2}(\operatorname{ch}\lambda x - 1)\right]_{\lambda=0} = \bar{\lambda}^2\frac{\operatorname{sh}\lambda x}{2} = 0$$

resulting for $a = 1$. Furthermore, according to (33)

$$\mu\lambda = -\bar{\lambda}\cot\bar{\lambda}l$$

and consequently,

$$\left[\frac{\mu}{\lambda^2}\right]_{\lambda=0} = -\left[\frac{\bar{\lambda}\cot\bar{\lambda}l}{\lambda^3}\right]_{\lambda=0} = -\infty.$$

The third term in the expression for y and through it value y itself becomes ∞. Thus the curves (fig. 5) have a point of discontinuity when $a = 1$ or, in other words, the original bar form is undefined for $a = 1$, so that the case $a = 1$ must be excluded from the investigations.

Figure 6 gives the original bar form (corresponding to (46)) for $a = 0$ at exaggerated scale. We use it as original form. We now reduce the bar forms resulting from (46) for different a in such a manner that the maximum ordinates (= ordinates for $x = l$) agree for all a values with the maximum ordinates for $a = 0$. By virtue of (32) and (33), (46) gives the maximum ordinate at

$$y_{max} = \epsilon\left(\frac{\bar{\lambda}^2}{\lambda^2} + 1\right)(1 + \mu\lambda l) \qquad (47)$$

Let $\epsilon = \epsilon_o$ for $a = 0$; then, because of

$$\overline{\lambda}_o \, l = \lambda_o \, l \sim \frac{5}{4} \pi \quad \text{and} \quad \mu_o \sim - 1$$

it gives

$$[y_{max}]_{a=0} \cong 2 \, \epsilon_o \left(1 - \frac{5}{4} \pi\right) = - 5.86 \, \epsilon_o \tag{48}$$

To assure the same value of y_{max} for other values of a also, we put:

$$\epsilon = - \frac{5.86 \, \epsilon_o}{\left(\frac{\overline{\lambda}^2}{\lambda^2} + 1\right)(1 + \mu \, \lambda \, l)} = - \frac{5.86}{1 + \mu \, \lambda \, l} \frac{1 - a}{2 - a} \epsilon_o \tag{49}$$

Figure 7 shows the reduction factor $\frac{\epsilon}{\epsilon_o}$ against a. With this choice of ϵ, (46) manifests bar forms for different a which practically do not deviate from each other, as seen in figure 8, where $- y/\epsilon_o$ for $x = l$, $x = \frac{3}{4} l$ and $x = \frac{1}{2} l$ proportional to the ordinates of the reduced bar form[2] are plotted against a. The discrepancies of the curves for $x = \frac{3}{4} l$ and $x = \frac{1}{2} l$ from a line parallel with the axis of abscissas are very minute. The greatest percentage of discrepancy of the ordinates among each other obviously occurs when $\frac{x}{l} < \frac{1}{2}$, which is not shown in the graph. In the range of $0 \leq a < 1.09$ (higher a values should be of no practical interest) the maximum discrepancy among the $\frac{y}{\epsilon_o}$ ordinates amounts, for instance, for $x = \frac{1}{4} l$, to about 15 percent. Admittedly, the criterion of the approach is not this figure but the maximum error referred to the maximum ordinate. This, however, does not occur at low $\frac{x}{l}$, but at $\frac{x}{l} = \frac{3}{4}$ and in the range of $0 < a < 1.09$ is less than 2.5 percent, and in the range of $0 < a < 1.05$ even less than 1.6 percent.

This proves that bar forms chosen according to (46) and containing the ϵ value given in (39) show such little discrepancy as to render comparison of the computed results possible without committing any great errors.

3. Solution

With a view to (35), (44) gives for η_t:

$$\rho F \ddot{\eta}_t + E J \bar{\lambda}^4 (1 - a) \eta_t = a E J \bar{\lambda}^4 \epsilon \qquad (50)$$

There are three distinct cases:

(a) $a < 1$; (b) $a > 1$; (c) $a = 1$.

We confine ourselves to cases (a) and (b), as the bar form y is not defined for $a = 1$. (See VI,2.)

The physical interpretation of these cases is as follows: Let P_E = Eulerian buckling load, $\bar{\lambda}_E$ = corresponding $\bar{\lambda}$ value, and a_E = ratio of longitudinal load to Eulerian load. Then

$$a_E = - \frac{X}{P_E} = - \frac{X}{E J \bar{\lambda}_E^2} \qquad (51)$$

or, because of (28)

$$a_E = a \frac{\bar{\lambda}^2}{\bar{\lambda}_E^2} \qquad (52)$$

It is shown in VII,1 that $\bar{\lambda}_E$ agrees with the value of $\bar{\lambda}$ for $a = 1$; (52) is graphed in figure 9. For $a_E = 1$, it is $a = 1$, so that our two cases (a) and (b) may also be expressed as

$$a_E < 1 \quad \text{and} \quad a_E > 1.$$

Physically, this means:

The shock load is lower than the Eulerian load;

The shock load is higher than the Eulerian load.

a) Shock load lower than Eulerian load.- With the assumed initial conditions,

$$\eta_t = 0 \quad \text{and} \quad \dot{\eta}_t = 0 \quad \text{for} \quad t = 0$$

the resolution of (50) gives, analogous to the second Euler case in the Koning-Taub report (reference 1):

$$\eta_t = \frac{a}{1 - a} \epsilon (1 - \cos p t) \tag{53}$$

where

$$p = \bar{\lambda}^2 \sqrt{\frac{EJ}{\rho F}} \sqrt{1 - a} \tag{54}$$

is the frequency. With index 0 denoting the quantities referred to the free fundamental oscillation ($a = 0$), we have:

$$p = p_0 \frac{\bar{\lambda}^2}{\lambda_0^2} \sqrt{1 - a} \tag{55}$$

Figure 10 shows the ratio $\frac{p}{p_0}$ versus a_E for the fundamental oscillation. As in the second Euler case, the frequencies drop as the load increases and disappear altogether when $a = 1$.

Thus with (43) and (53) the resolution of (8):

$$\eta = \eta_t \eta_x = \frac{a}{1 - a} \epsilon (1 - \cos p t)$$

$$[\operatorname{ch} \lambda x - \cos \bar{\lambda} x + \mu(\operatorname{sh} \lambda x - \frac{\lambda}{\bar{\lambda}} \sin \bar{\lambda} x)] \tag{56}$$

At the end of the shock $t = \tau$, it is:

$$\eta = \frac{a}{1 - a} \epsilon (1 - \cos p\tau)$$

$$[\operatorname{ch} \lambda x - \cos \bar{\lambda} x + \mu(\operatorname{sh} \lambda x - \frac{\lambda}{\bar{\lambda}} \sin \bar{\lambda} x)] \tag{57}$$

$$\frac{\partial \eta}{\partial t} = \frac{a}{1 - a} \epsilon p \sin p\tau$$

$$[\operatorname{ch} \lambda x - \cos \bar{\lambda} x + \mu(\operatorname{sh} \lambda x - \frac{\lambda}{\bar{\lambda}} \sin \bar{\lambda} x)] \tag{58}$$

The free oscillation of the bar after the shock is with due allowance for (39):

$$\eta = \sum_n A_n \sin(p_{on} \bar{t} + \varphi_n)(\operatorname{ch} \lambda_{on} x - \cos \lambda_{on} x -$$

$$- \operatorname{sh} \lambda_{on} x + \sin \lambda_{on} x) \tag{59}$$

The choice of time coordinates τ after the shock is such that $\bar{t} = 0$ at the end of the actual shock period,

that is, the start of the free oscillation. Then $\bar{t} = t - \tau$ and the start of the free oscillations are according to (59):

$$\eta = \sum_n A_n \sin \varphi_n (\operatorname{ch} \lambda_{on} x - \cos \lambda_{on} x - \operatorname{sh} \lambda_{on} x + \sin \lambda_{on} x) \qquad (60)$$

$$\frac{\partial \eta}{\partial t} = \sum_n A_n p_{on} \cos \varphi_n (\operatorname{ch} \lambda_{on} x - \cos \lambda_{on} x - \operatorname{sh} \lambda_{on} x + \sin \lambda_{on} x) \qquad (61)$$

These values of the deflection and rate of deflection at the start of the free oscillation must agree with the corresponding values for the termination of the actual shock (57) and (58). To define the constants A_n and φ_n, in (59), we then have:

$$\sum_n A_n \sin \varphi_n \eta_{x_{on}} = \frac{a}{1 - a} \epsilon (1 - \cos p \tau) \eta_x \qquad (62)$$

$$\sum_n A_n p_{on} \cos \varphi_n \eta_{x_{on}} = \frac{a}{1 - a} \epsilon p \sin p \tau \eta_x \qquad (63)$$

Herein:

$$\eta_{x_{on}} = \operatorname{ch} \lambda_{on} x - \cos \lambda_{on} x - \mu_{on} (\operatorname{sh} \lambda_{on} x - \sin \lambda_{on} x) =$$

$$= \frac{1}{2} \left[e^{\lambda_{on} x} (1 + \mu_{on}) + e^{-\lambda_{on} x} (1 - \mu_{on}) - e^{i\lambda_{on} x} (1 - \mu_{on} i) - e^{-i\lambda_{on} x} (1 + \mu_{on} i) \right] \qquad (64)$$

is the nth natural function of the free bar oscillation,* and again by omitting index 1:

$$\eta_x = \operatorname{ch} \lambda x - \cos \bar{\lambda} x + \mu \left(\operatorname{sh} \lambda x - \frac{\lambda}{\bar{\lambda}} \sin \bar{\lambda} x \right) =$$

$$\frac{1}{2} \left[e^{\lambda x} (1 + \mu) + e^{-\lambda x} (1 - \mu) - e^{i\bar{\lambda} x} \left(1 - \mu \frac{\lambda i}{\bar{\lambda}}\right) - e^{-i\bar{\lambda} x} \left(1 + \mu \frac{\lambda i}{\bar{\lambda}}\right) \right] \qquad (65)$$

*Simplification of $\mu_{on} \sim -1$ is purposely foregone, since the exact value of $\eta_{x_{on}}$ in the ensuing series development affords more simple results than the inaccurate one.

the first natural function of the bar oscillation in presence of a longitudinal force.

The system $\eta_{x_{on}}$ is orthogonal and any function may be expanded in convergent series conformably. (See V,1.)

Equations (62) and (63) in conjunction with multiplication of $\eta_{x_{on}}$ and integration of $x = 0$ to l, give:

$$A_n \sin \varphi_n = \frac{a}{1-a} \epsilon (1-\cos p\tau) \frac{\int_0^l \eta_{x_{on}} \eta_x \, dx}{\int_0^l \eta_{x_{on}}^2 \, dx} \tag{66}$$

$$A_n \cos \varphi_n = \frac{a}{1-a} \epsilon \frac{p}{p_{on}} \sin p\tau \frac{\int_0^l \eta_{x_{on}} \eta_x \, dx}{\int_0^l \eta_{x_{on}}^2 \, dx} \tag{67}$$

The addition of the squares of these terms gives the coefficients of the series expansion at

$$A_n = \frac{a}{1-a} \epsilon \sqrt{(1-\cos p\tau)^2 + \frac{p^2}{p_{on}^2} \sin^2 p\tau} \frac{\int_0^l \eta_{x_{on}} \eta_x \, dx}{\int_0^l \eta_{x_{on}}^2 \, dx} \tag{68}$$

and the division of (66) by (69) gives the phase displacement φ_n at

$$\tan \varphi_n = \frac{p_{on}}{p} \frac{1 - \cos p\tau}{\sin p\tau} \tag{69}$$

The evaluation of the integrals is best effected with the exponential form of the functions $\eta_{x_{on}}$ and η_x. Omitting the n indices, we have:

$$\int_0^l \eta_{x_o} \eta_x \, dx = \left\{ \frac{1}{4} (1+\mu_o) e^{\lambda_o x} \left[\frac{1+\mu}{\lambda+\lambda_o} e^{\lambda x} - \frac{1-\mu}{\lambda-\lambda_o} e^{-\lambda x} - \right. \right.$$

$$\left. \left. - \frac{1-\mu \frac{\lambda i}{\bar{\lambda}}}{i\bar{\lambda} + \lambda_o} e^{i\bar{\lambda}x} + \frac{1+\mu \frac{\lambda i}{\bar{\lambda}}}{i\bar{\lambda} - \lambda_o} e^{-i\bar{\lambda}x} \right] +$$

$$+(1-\mu_o)e^{-\lambda_o x}\left[\frac{1+\mu}{\lambda-\lambda_o}e^{\lambda x}-\frac{1-\mu}{\lambda+\lambda_o}e^{-\lambda x}-\right.$$

$$\left.-\frac{1-\mu\,\frac{\lambda i}{\bar{\lambda}}}{i\bar{\lambda}-\lambda_o}e^{i\bar{\lambda}x}+\frac{1+\mu\,\frac{\lambda i}{\bar{\lambda}}}{i\bar{\lambda}+\lambda_o}e^{-i\bar{\lambda}x}\right]+$$

$$-(1-\mu_o i)e^{i\lambda_o x}\left[\frac{1+\mu}{\lambda+\lambda_o i}e^{\lambda x}-\frac{1-\mu}{\lambda-\lambda_o i}e^{-\lambda x}-\right.$$

$$\left.-\frac{1-\mu\,\frac{\lambda i}{\bar{\lambda}}}{i(\bar{\lambda}+\lambda_o)}e^{i\bar{\lambda}x}+\frac{1+\mu\,\frac{\lambda i}{\bar{\lambda}}}{i(\bar{\lambda}-\lambda_o)}e^{-i\bar{\lambda}x}\right]-$$

$$-(1+\mu_o i)e^{-i\lambda_o x}\left[\frac{1+\mu}{\lambda-\lambda_o i}e^{\lambda x}-\frac{1-\mu}{\lambda+\lambda_o i}e^{-\lambda x}-\right.$$

$$\left.\left.-\frac{1-\mu\,\frac{\lambda i}{\bar{\lambda}}}{i(\bar{\lambda}-\lambda_o)}e^{i\bar{\lambda}x}+\frac{1+\mu\,\frac{\lambda i}{\bar{\lambda}}}{i(\bar{\lambda}-\lambda_o)}e^{-i\bar{\lambda}x}\right]\right\}_o^l$$

Taking into consideration (32), (33) expressed in exponential form:

$$e^{\lambda l}(1+\mu)+e^{-\lambda l}(1-\mu)=0 \tag{70}$$

$$e^{i\bar{\lambda}l}\left(1-\mu\,\frac{\lambda i}{\bar{\lambda}}\right)+e^{-i\bar{\lambda}l}\left(1+\mu\,\frac{\lambda i}{\bar{\lambda}}\right)=0 \tag{71}$$

and the corresponding terms for function $\eta_{x_{on}}$:

$$e^{\lambda_o l}(1+\mu_o)+e^{-\lambda_o l}(1-\mu_o)=0 \tag{72}$$

$$e^{i\lambda_o l}(1-\mu_o\, i)+e^{-i\lambda_o l}(1+\mu_o\, i)=0 \tag{73}$$

The integral in the numerator of (68) reduces to

$$\int_o^l \eta_{x_o}\,\eta_x\,dx = 2\lambda_o^2(\lambda\mu-\lambda_o\mu)\left(\frac{1}{\lambda_o^4-\lambda^4}-\frac{1}{\lambda_o^4-\bar{\lambda}^4}\right).$$

The integral in the denominator of (68) is:

$$\int_0^l \eta_{x_0}^2 \, dx = \frac{1}{2\lambda_0}\left\{\frac{1}{4}\left[(1+\mu_0)^2 \, e^{2\lambda_0 x} - (1-\mu_0)^2 \, e^{-2\lambda_0 x} - \right.\right.$$

$$- (1-\mu_0 i)^2 \, i \, e^{2i\lambda_0 x} + (1+\mu_0 i)^2 \, i \, e^{-2i\lambda_0 x}\Big] +$$

$$+ \left[2\lambda_0 x - \frac{(1+\mu_0)(1-\mu_0 i)}{1+i} e^{(1+i)\lambda_0 x} + \right.$$

$$+ \frac{(1-\mu_0)(1-\mu_0 i)}{1-i} e^{(1-i)\lambda_0 x} -$$

$$- \frac{(1+\mu_0)(1+\mu_0 i)}{1-i} e^{(1-i)\lambda_0 x} +$$

$$\left.\left. + \frac{(1-\mu_0)(1+\mu_0 i)}{1+i} e^{-(1+i)\lambda_0 x}\right]\right\}_0^l$$

With a view to (72) and (73) this expression reduces to:

$$\int_0^l \eta_{x_0}^2 \, dx = l.$$

The coefficients of the series are obtained from

$$A_n = \frac{2a}{1-a} \epsilon \frac{\lambda_{on}^2}{l} (\lambda\mu - \lambda_{on}\mu_{on}) \left(\frac{1}{\lambda_{on}^4 - \lambda^4} - \right.$$

$$\left. - \frac{1}{\bar{\lambda}_{on}^4 - \bar{\lambda}^4} \right) \sqrt{(1 - \cos p\tau)^2 + \frac{p^2}{p_{on}^2} \sin^2 p\tau} \qquad (74)$$

At this time it is pointed out that all formulas developed in this section can be forthwith generalized for the case of any original bar form by simply inserting the $\sum_n$ sign at the right-hand side of (42) to (46), (56), (59), (62), (63), (66), (68), and (74), and giving $\lambda, \bar{\lambda}, \mu$ and p the index n. n = 1,2,3,... correspond to the fundamental oscillation, first, second, ... to the upper oscillation. However, for the reasons advanced in VI,1, the investigation is confined to our specially selected bar form.

Referring the shock period τ to the oscillation period T of the free fundamental oscillation, we obtain with

$$\tau = b\,T = \frac{2\,\pi}{p_{o1}}\,b \tag{75}$$

and with due consideration to (55):

$$p\,\tau = 2\,\pi\,b\,\frac{\bar{\lambda}^2}{\lambda_{o1}^2}\sqrt{1 - a} \tag{76}$$

This enables us to compute the coefficients A_n for different a and b from (74). (See table I.) The a values denote the magnitude of the shock load and the b values the shock period.

The maximum b values are those at which the time function of (57) reaches first its maximum, i.e., at which the maximum deflections are reached during the shock. This occurs according to (57) for $p\tau = \pi$, or according to (76) when

$$b = \frac{\lambda_{o1}^2}{\bar{\lambda}^2}\,\frac{1}{2\sqrt{1 - a}} \tag{77}$$

The shock period b from (77) is plotted against a_E in figure 16. Given the coefficients for the range $0 < p\tau < \pi$ they are known for any values of $p\tau$, inasmuch as they are periodic in $p\tau$.

The figures $100\,\frac{A_n}{A_1}$ cited in the last three columns of table I give the amount of the particular coefficient in percent of the first coefficient. The coefficients are seen to converge very rapidly for small a and b values and somewhat more slowly for high a and b values. In the range of $0 < a < 0.50$ the first three coefficients suffice. The amount of the third coefficient is, at the most, 0.3 percent of the first coefficient. In the $0.5 < a < 0.99$ range the first four coefficients are sufficient. The fourth coefficient is, at the most, 0.2 percent of that of the first. For computing the deflections even a lower coefficient would suffice, but for computing the moments the coefficients of higher order grow in significance as their factors λ_{on}^2 increase with n.

We show in table II the phase displacements φ_n as computed from (69).

Taken absolute the maximum moment is decisive for the estimation of the behavior of the bar in buckling due to shock load.. The $1/EJ$ time moments during the actual shock period are, according to (56):

$$\frac{\partial^2 y}{\partial x^2} = \frac{a}{1-a}\,\epsilon\,\bar{\lambda}^2\,(1-\cos p\,t)\left[\frac{\lambda^2}{\bar{\lambda}^2}\,\mathrm{ch}\,\lambda x + \cos\bar{\lambda}x + \mu\left(\frac{\lambda^2}{\bar{\lambda}^2}\,\mathrm{sh}\,\lambda x + \frac{\lambda}{\bar{\lambda}}\sin\bar{\lambda}x\right)\right] \tag{78}$$

and after the actual shock period according to (59):

$$\frac{\partial^2 y}{\partial x^2} = \sum_n A_n\,\lambda_{on}^2 \sin\left[p_{on}(t-\tau)+\varphi_n\right](\mathrm{ch}\,\lambda_{on}x+\cos\lambda_{on}x - \mathrm{sh}\,\lambda_{on}x-\sin\lambda_{on}x) \tag{79}$$

The maximum curvature $\frac{\partial^2\eta}{\partial x^2}$ now occurs either during or after the actual shock period. It can occur during the actual shock only when the period lasts until the highest possible deflection is reached, that is, when b has at least reached the value given in (77). If this happens the time maximum of the term denoting the period during shock is, according to (78) and (36):

$$\max\frac{\partial^2 y}{\partial x^2} = \frac{2\,a}{1-a}\,\epsilon\,\bar{\lambda}^2\left[(1-a)(\mathrm{ch}\,\lambda x+\mu\,\mathrm{sh}\,\lambda x)+\cos\bar{\lambda}x+\mu\sqrt{1-a}\sin\bar{\lambda}x\right] \tag{80}$$

The place maximum of $\frac{\partial^2\eta}{\partial x^2}$ (taken absolute) occurs when the place function $\frac{d^2\eta_x}{dx^2}$, that is, the bracketed term in (80) reaches its maximum or minimum. The maximum of $(1-a)(\mathrm{ch}\,\lambda x+\mu\,\mathrm{sh}\,\lambda x)$ is reached when $x=0$, because $\mu<0$. Besides, since according to figure 11, $\mu\sqrt{1-a}$ is a true negative fraction, positive

$$\cos\bar{\lambda}x+\mu\sqrt{1-a}\sin\bar{\lambda}x$$

can only occur within the lengths

$$0 < \bar{\lambda}\, x < \frac{\pi}{2}$$

and

$$\frac{5}{4}\pi < \bar{\lambda}\, x < \bar{\lambda}\, l = 4.5 \quad \text{approximately.}$$

Within these lengths the maximum of

$$\cos \bar{\lambda} x + \mu \sqrt{1 - a} \sin \bar{\lambda} x$$

likewise occurs at $x = 0$. The maximum of $\frac{d^2\eta_x}{dx^2}$ thus occurs at $x = 0$ and equals $2 - a$. Figure 12 shows the maximum $\frac{d^2\eta_x}{dx} = 2 - a$ plotted against a. The minimum of the place function $\frac{d^2\eta_x}{dx^2}$ lies in the zone of $\cos \bar{\lambda}x < 0$ and $\sin \bar{\lambda}x > 0$, that is, $\frac{\pi}{2} < \bar{\lambda}x < \pi$. It is more easily found when assuming that the effect of the two hyperbolic terms of $\frac{d^2\eta_x}{dx^2}$ is small against the two trigonometrical terms when approaching the minimum. From

$$\frac{d}{dx}(\cos \bar{\lambda}\, x + \mu \sqrt{1 - a} \sin \bar{\lambda}\, x) =$$

$$= \bar{\lambda}^2 (- \sin \bar{\lambda}\, x + \mu \sqrt{1 - a} \cos \bar{\lambda}\, x) = 0$$

the minimum is then obtained in the neighborhood of

$$\bar{\lambda}\, x = \tan^{-1} \mu \sqrt{1 - a}$$

The computed minima of place function $\frac{d^2\eta_x}{dx^2}$, taken absolute, are shown in figure 12. (The figures lie around $\frac{x}{l} = 0.65$.) They are seen to be lower than the maximum values for $0 < a < 0.975$, so that in this range the maximum $\frac{\partial^2\eta}{\partial x^2}$ occurs at $x = 0$. For $1 > a > 0.975$ the minimum of $\frac{d^2\eta_x}{dx^2}$ is decisive. For $a = 0.99$ its absolute value is only 1.8 percent lower than the maximum for the same a value, so the assumed absolute maximum of the moment <u>during</u> the actual shock period will be accurate enough for all $a \leq 0.99$ and $b \geq \frac{\lambda_{01}^2}{\bar{\lambda}^2} \frac{1}{2\sqrt{1-a}}$ when made propor-

tional to $\left|\frac{\partial^2\eta}{\partial x^2}\right|_{max} = 2\,\frac{a(2-a)}{1-a}\,\epsilon\,\bar{\lambda}^2$, or because of (49), to

$$\left|\frac{\partial^2\eta}{\partial x^2}\right|_{max} = -\,11.72\cdot\frac{a\bar{\lambda}^2}{1+\mu\,\lambda}\,\epsilon_o \qquad (81)$$

The maximum of $\frac{\partial^2\eta}{\partial x^2}$ after the actual shock period must be defined by trial from (79) which, although not unduly difficult for a specific case, requires nevertheless a large amount of paper work for such general investigations as the present report. For this reason we determine only the upper limit value for maximum $\partial^2\eta/\partial x^2$.

The place-maximum of the individual $\eta_{x_{on}}$ in (79) is 2 and occurs with $x = 0$. The time-maximum or minimum of $\sin[p_{on}(t-\tau)+\varphi_n]$ is ± 1. As the A_n coefficients, with the exception of the first, are negative, the assumed absolute maximum of (79) cannot exceed

$$\left|\frac{\partial^2\eta}{\partial y^2}\right|_{max} = 2\left[A_1\,\lambda_{o1}^2 - \sum_{n=2}^{\infty} A_n\,\lambda_{on}^2\right] \qquad (82)$$

The upper maximum in (82) is almost reached, at least theoretically, according to the following. With due consideration to λ_{on} (see V,2,b), (55) gives the ratio of frequencies of the (n-1)th free higher oscillation to the free fundamental oscillation almost exactly at

$$\frac{p_{on}}{p_{o1}} = \frac{(4n+1)^2}{25}.$$

Within the period of 25 free fundamental oscillations, the bar thus executes almost precisely:

	81	1st	free higher	oscillations	
	169	2d	"	"	"
and	289	3d	"	"	"

that is, produces a beat whose period is 25 T. Within the time interval of 12.5 T after the actual shock the value $\max\left|\frac{\partial^2\eta}{\partial x^2}\right|$ thus reaches its minimum deviation once relative to its upper maximum (82). In view of the great number of oscillation combinations during this interval and the fact

that the frequencies increase with n, it may be assumed that the maximum of $\left|\frac{\partial^2 \eta}{\partial x^2}\right|$ occurs at an instant in which almost or exactly

$$\sin [p_{o1} (t - \tau) - \varphi_1] = \pm 1$$

and $$\sin [p_{on} (t - \tau) - \varphi_n] = \mp 1$$ are valid.

Here it should be pointed out that in reality certain discrepancies from the theoretical upper limit value given in (82) are nevertheless to be expected; that is, in the cases in which the theoretical minimum discrepancy from it would occur only after a greater number of fundamental oscillations. For, in fact, the degree of damping is already appreciable and reduces the amplitudes. However, we pass over the damping effect, as stated in the beginning.

The cases in which the maximum $\frac{\partial^2 \eta}{\partial x^2}$ and those in which its upper limit value <u>after</u> the actual shock are decisive, are analyzed in VII,2.

b) Shock Load Greater than Eulerian Load

<u>$a > 1$; $(a_E > 1)$</u>

With the initial conditions $\eta_t = 0$, $\dot{\eta}_t = 0$ for $t = 0$, the solution in this case is analogous to the second Euler case (reference 1):

$$\eta_t = \frac{a}{1 - a} \epsilon (\operatorname{ch} p\, t - 1) \tag{83}$$

where

$$p = \overline{\lambda}^2 \sqrt{\frac{EJ}{\rho F}} \sqrt{a - 1} = p_o \frac{\overline{\lambda}^2}{\overline{\lambda}_o^2} \sqrt{a - 1} \tag{84}$$

The course of the further investigation agrees with that for $a < 1$. The equation of the elastic line for the actual shock period $(t \leqq \tau)$ is:

$$\eta = \frac{a}{a - 1} \epsilon (\operatorname{ch} p\, t - 1)\, \eta_x \tag{85}$$

At the end of the shock $(t = \tau)$, we have:

$$\eta = \frac{a}{a - 1} \epsilon \, (\mathrm{ch}\ p\tau - 1)\, \eta_x \tag{86}$$

$$\frac{\partial \eta}{\partial t} = \frac{a}{a - 1} p \ \mathrm{sh}\ p\tau \ \eta_x \tag{87}$$

whereby η_x is given in (65).

For the condition after the shock $(t \geqq \tau)$ (59) and for $t = \tau$ (60) and (61) are applicable.

The A_n coefficients and the phase displacement φ_n of the series (59) are obtained when equating the right-hand sides of (86) and (60), respectively, (87) and (61) with

$$A_n = \frac{2\,a}{a - 1} \epsilon \frac{\lambda_{on}^2}{l} (\lambda\mu - \lambda_{on}\,\mu_{on})$$

$$\left(\frac{1}{\lambda_{on}^4\,\lambda^4} - \frac{1}{\lambda_{on}^4\,\bar{\lambda}^4}\right) \sqrt{(\mathrm{ch}\ p\tau - 1)^2 + \frac{p^2}{p_{on}^2} \mathrm{sh}^2\ p\tau} \tag{88}$$

and

$$\tan \varphi_n = \frac{p_{on}}{p} \frac{\mathrm{ch}\ p\tau - 1}{\mathrm{sh}\ p\tau} \tag{89}$$

making

$$p\tau = 2\pi\, b \frac{\bar{\lambda}^2}{\lambda_{o1}^2} \sqrt{a - 1} \tag{90}$$

applicable because of (87) and (84).

The A_n coefficients have been tabulated for different shock loads (a) and periods (b) in table III. The $100\,\frac{A_n}{A_1}$ figures in the last three columns give the amount of the respective coefficient in percent of the first coefficient.

The coefficients converge quite well, and so much the closer as a and b are smaller. The first four terms suffice throughout the range investigated. The amount of the fourth coefficient is, at the most, 2 percent of that of the first.

Table IV gives φ_n for different a and b.

The time function in (85) being aperiodic, the maximum deflection during the actual shock period is always reached with $t = \tau$. This instant, however, is also given by (59) which decides the condition after the shock. Bearing in mind that, contrary to range $a < 1$, the time function of the speed (87) is always positive at the instant the shock stops and that, therefore, the deflections and moments continue after the end of the shock, it is readily seen that the maximum moment always occurs after the actual shock; consequently, the investigation may be restricted to that of the $1/EJ$-fold moments of (79).

As concerns the upper limit value of (79), the same arguments and the same formulas are applicable as for $a < 1$, that is, the upper limit value of (79) is given by (82). It occurs at $x = 0$ in spite of the fact that - as seen in figure 12 - for $a > 1$ at the instant of incipient free oscillations the maximum value of the moment for $x = 0$ is smaller than its assumed absolute minimum value occurring at around $x = 0.65\ l$.

VII. RESULTS AND INTERPRETATION

1. Comparison with Static Case

The obvious criterion of the magnitude of moments in buckling due to shock loads is the moment of the same bar in static buckling stress. For this reason we shall at first, attempt to resolve the differential equation for static buckling of a bar of prescribed form. Thus we effect the calculation for the bar conformably to (46), for example, although it could be given direct for this particular case, as shown elsewhere.

The differential equation of static buckling is afforded from (8) when omitting the term with $\partial^2 y/\partial t^2$, although figure 13 reveals it even more elementary. It is

$$M = P\ (\eta + y - y_{max}) - \underline{A}\ (l - x)$$

and consequently,

$$\frac{\partial^2 \eta}{\partial x^2} + \frac{P}{EJ}\,\eta = \frac{1}{EJ}\,[\underline{A}\ (l - x) - P\ (y - y_{max})] \qquad (91)$$

The homogeneous equation,

$$\frac{\partial^2 \eta}{\partial x^2} + \frac{P}{EJ} \eta = 0 \tag{92}$$

resolves to

$$\eta = c_1 \cos \omega x + c_2 \sin \omega x \tag{93}$$

Putting (93) in (92) gives:

$$\omega^2 = \frac{P}{EJ}$$

and consequently,

$$\omega^2 = \overline{\lambda}^2 - \lambda^2 \tag{94}$$

because of (16) and $P = -X$. Equation (91) is resolved by variation of the constants in (93), that is, from

$$\eta = c_1(x) \cos \omega x + c_2(x) \sin \omega x \tag{95}$$

where

$$c_1(x) = \int_0^x \frac{f(x)\, u_2\, dx}{u_1'\, u_2 - u_2'\, u_1} + k_1$$

$$c(x) = \int_0^x \frac{f(x)\, u_1\, dx}{u_2'\, u_1 - u_1'\, u_2} + k_2$$

$$f(x) = \frac{1}{EJ} [\underline{A} (l - x) - P (y - y_{max})]$$

$$u_1 = \cos \omega x$$

$$u_2 = \sin \omega x$$

and k_1 and k_2 are constant values. The terms for y and y_{max} are taken from (46) and (47). After appropriate reductions and calculation of c_1 and c_2, it gives

$$\eta = \frac{A}{P}\left(l - x - l\cos\omega x - \frac{1}{\omega}\sin\omega x\right) -$$

$$- y + y_{max}(1 - \cos\omega x) - \epsilon\left[\operatorname{ch}\lambda x + \frac{\bar{\lambda}^2}{\lambda^2}\cos\bar{\lambda} x + \right.$$

$$\left. +\mu\left(\operatorname{sh}\lambda x + \frac{\bar{\lambda}}{\lambda}\sin\bar{\lambda} x\right) - \left(\frac{\bar{\lambda}^2}{\lambda^2} + 1\right)\left(\frac{\mu\lambda}{\omega}\sin\omega x + \cos\omega x\right)\right]$$

$$+ k_1\cos\omega x + k_2\sin\omega x \qquad (96)$$

The boundary condition $\eta = 0$ for $x = 0$ gives $k_1 = 0$; those of $\frac{d\eta}{dx} = x = 0$ and $\eta = 0$ for $x = 0$ and $x = l$ give two equations for $\frac{A}{P}$ and k_2, thus yielding with allowance for (32) and (33):

$$k_2 = \frac{2}{\omega}\frac{A}{P}$$

and

$$\frac{A}{P} = -\mu\lambda\epsilon\left(\frac{\bar{\lambda}^2}{\lambda^2} + 1\right)$$

The introduction of the values of k_1, k_2, and $\frac{A}{P}$ in (96) with consideration to (36) and (94) gives:

$$\eta = \epsilon\frac{a}{1 - a}\left[\operatorname{ch}\lambda x - \cos\bar{\lambda} x + \mu\left(\operatorname{sh}\lambda x - \frac{\lambda}{\bar{\lambda}}\sin\bar{\lambda} x\right)\right] \qquad (97)$$

This term approaches ∞ as a approaches the value 1. Consequently, the Eulerian buckling load occurs at $a = \frac{P}{EJ\bar{\lambda}^2} = 1$, as already explained in VI,3. Since then, $\bar{\lambda} l = 4.5$ (about) according to figure 4, we obtain for the Eulerian load the known value

$$P_E \cong 4.5^2\frac{EJ}{l^2} \cong 2\pi^2\frac{EJ}{l^2} \qquad (98)$$

independent from the original bar form.

The $1/EJ$-fold moments are obtained in first approximation from (97) at

$$\frac{d^2\eta}{dx^2} = \epsilon \frac{a}{1-a} \bar{\lambda}^2 \left[\frac{\lambda^2}{\bar{\lambda}^2} \operatorname{ch} \lambda x + \cos \bar{\lambda} x + \right.$$

$$\left. + \mu \left(\frac{\lambda^2}{\bar{\lambda}^2} \operatorname{sh} \lambda x + \frac{\lambda}{\bar{\lambda}} \sin \bar{\lambda} x \right) \right] \qquad (99)$$

Comparison with (80) reveals them to be exactly half as high as the time maximum of the 1/EJ-fold moments due to shock load by a time-constant force, for an effective period equal to half the period of the oscillations accompanying this load.*

This result could equally have been obtained direct: The solution (43) of (8) represents at the same time the resolution of (8) without the $\rho F \frac{\partial^2 \eta}{\partial t^2}$ term, when equating $\eta_t = k = \text{constant}$. Then (44) becomes:

$$[(E J \bar{\lambda}^2 + X) \bar{\lambda}^2 k + X \epsilon \bar{\lambda}^2] \eta_x = 0,$$

hence,

$$k = - \frac{\epsilon X}{E J \bar{\lambda}^2 + X} = \frac{a}{1-a} \epsilon$$

Or, by the same argument, so long as the shock force is constant in time and lower than the Eulerian load, the oscillations are harmonic. If the bar form is such as to insure only one definite oscillation - in the present case, the fundamental - the mean position of the oscillation corresponds to the equilibrium position assumed by the bar under static load. The mean position is reached after a one fourth period; the position of potential total energy and consequently of maximum deflections and moments is reached after one half period. The oscillation being harmonic, the maximum deflections and moments are exactly twice as great as the corresponding magnitudes in the mean position.

In the general case, however, with the bar form such as to produce a motion consisting of the superposition of several normal oscillations, the motion of the individual

---

*That stresses due to "sudden" loads can become twice as high as in static loading, is a well-known fact. (Poncelet, Introduction a la Mecanique industrielle, physique et experimentale, 1830.)

bar particles is not synchronous, nor is there any condition in which the total energy has potential form. In this case then there is no simple relationship between the deflections and moments produced during the period of loading due to static and to "sudden" loading.* The deflections and moments for the static case are then obtained from the corresponding magnitudes of the static case by substituting $\frac{a}{1-a}\epsilon_n$ for the time function η_{tn}, or by direct treatment of the static case.

These considerations referred to cases of tension lower than the Eulerian load ($a < 1$). For tensions greater than the Eulerian load ($a < 1$) the approximate equation of the elastic line fails, as known (curvature = d^2y/dx^2). For such cases the exact equation should be used, i.e., write:

$$\frac{\frac{d^2\eta}{dx^2}}{\left(\sqrt{1+\left(\frac{d\eta}{dx}\right)^2}\right)^3} + \frac{P}{EJ}\eta = \frac{1}{EJ}\left[\underline{A}(l-x) - P(y-y_{max})\right] \qquad (100)$$

instead of (91).

The resolution of (100) is very difficult. Even a second approximation as attempted by Trefftz (reference 5) seems intractable in view of the complicated interference function of (100). Added to this is the fact that when effecting the dynamic analysis, we also substituted its first approximative value $d^2\eta/dx^2$ for the curvature. A comparison of the results of the dynamic study obtained in first approximation with those of the static study in second approximation would, however, not be logical.

---

*These explanations are, according to Section 128 of Love-Timpe's volume on elasticity. It states, among other things that, in the general case "The distortion remains less than twice the distortion existing in equilibrium position." This does not seem strictly valid. It is well possible that at isolated points the distortion may be greater than the twofold distortion existing in static equilibrium position, even if the energy of the whole bar, which is governed by an integral term along the bar, is not purely potential at any instant. (Compare VII,2 of this report, which contains similar deductions for the free oscillations following the actual shock.)

Under these circumstances we content ourselves with comparing the static to the dynamic case for $a < 1$, while for evaluating the results of the dynamic case for $a > 1$, we only adduce that of the dynamic case for $a < 1$ in comparison.

2. Numerical Comparison, Deductions, and Examples

On the basis of the foregoing, the function for the moment in the static case for $a < 1$ is, according to (81):

$$\left|\frac{d^2 y}{dx^2}\right|_{max} = - 5.86 \frac{a \bar{\lambda}^2}{1 + \mu \lambda l} \epsilon_o \qquad (101)$$

The ratio of the maximum moments (taken absolute) in the static and dynamic case is then, according to (81) and (101) for $a < 1$:

$$c = 2 \qquad (102)$$

a) Provided the maximum moment occurs during the actual shock, and

b) Provided the upper limit of c is according to (82) and (101):

$$c = - \frac{0.342(1 + \mu \lambda l)}{\epsilon_o a \lambda^2} [A_1 \lambda_{o1}^2 - \sum_{n=2}^{\infty} A_n \lambda_{on}^2] \qquad (103)$$

From (102) and (103) it is seen that in our case the assumed absolute ratio of the decisive moments in the dynamic and static case is independent of the amount of original eccentricity ϵ_o (A_n/ϵ_o does not contain ϵ_o).

The evaluation of (103) affords the figures 14 to 20. The particular tables have been omitted. Suffice it to say that taking into account the terms of the series expansion applied in table I, the amount of the term of maximum order is, at the most, 2 percent of that of the first term.

Figure 17 gives the c values as ordinates, the b values as abscissas in logarithmic scale. The a and a_E values (in parenthesis) are the parameters. The range of each curve was chosen so that the maximum shock period (b) corresponds to the maximum deflection during the actual shock period. (b_{max} then corresponds to (77).)

According to figure 14 the stresses in short shock periods are lower than for an identical static stress. But at longer shock periods the static stresses can be exceeded considerably.

The maximum c values occur at shock periods corresponding to (77). They are, on the whole, greater than the maximum c value of (102) for the same shock period. Therefore, the maximum moments are even then only to be expected after the actual shock period, when the greatest deflection possible in this period is reached during the actual shock period.

This somewhat confusing statement needs further explanation. If the actual shock lasts just long enough to ensure the greatest deflection so that, as in our case only one definite normal oscillation occurs, then the total energy at the end of the shock is existent in the form of deformation energy. During the free oscillations* following the shock there is, therefore, no instant in which the energy of deformation is greater than at the instant of shock termination. Generally the first is even consistently lower than the latter for, aside from the type of support according to the second Euler case, there is no integral ratio between fundamental and upper oscillation frequency, hence no instant during the free oscillations in which the total energy is potential.

The result, according to which the upper boundary value of the maximum moments after the shock is greater than during the shock at the moment of maximum deflection, is, however, readily understood when bearing in mind that the highest moment in a certain period does not necessarily have to occur at the instant when the total energy is energy of deformation. Rather, there may be instants in which the superposition of oscillations may even induce still higher moments, even though the concurrently existing deformation energy of the whole bar - which, as is known, is proportional to the integral of the square of the moment - is lower than the deformation energy at the end of the shock.

Figure 15, which is simply the modified figure 14, reveals that in the range of higher shock loads the dynamic stresses pertaining to the same shock periods increase more slowly with increased shock load than the corresponding static stresses (and vice versa).

---

*Excepting the second Euler case, several free oscillations occur as a rule after the shock even when only one definite oscillation existed during the shock.

Contrariwise, figure 16 shows that the greatest possible c values increase with the shock loads whereby, however, the shock periods (b) for these values increase equally. In our case, when the shock period is long enough, the dynamic load may reach around 3.4 times that of the static stress, whereas with vanishing shock load the stress is at the most, twice as high as the static stress.

Figure 17 shows the shock periods (b) against shock load (a_E) for shock stress equal to static stress. These shock periods are seen to increase slowly at first, then faster, and to approach infinity in the neighborhood of the Eulerian load.

Figure 18 shows c against shock period for $a_E = 0.770$, together with periods exceeding those of (77). After becoming maximum, c at first drops with increasing shock period but can, of course, not drop below 2, since this figure had already been reached once at the instant of maximum deflection during the shock. Thus, starting from a stated shock period $c = 2$ is valid. At still longer shock periods, c then increases again, etc. At other a_E values, the trend of the curve is quite similar.

To render the interpretation of the dynamic test data possible in the $a > 1$ range, in view of the absence of comparative base of static case, we plotted the dimensionless quantities:

$$\frac{l^2}{\epsilon_o}\left|\frac{\partial^2\eta}{\partial x^2}\right|_{max} = \frac{2\,l^2}{\epsilon_o}\left[A_1\,\lambda_{o1}^2 - \sum_{n=2}^{\infty} A_n\,\lambda_{on}^2\right]$$

(see (82)), which are proportional to the upper boundary values of the moments for the whole investigated range of a and a_E against b in figure 19, with a and a_E as parameters, abscissas and ordinates being given in logarithmic scale to ensure better survey. Figure 20 gives the same results, but b serves as parameter and the a_E values form the abscissas.

According to figure 22, there is no maximum moment when $a \geq 1$; the moments continue to increase with the shock period, while for $a < 1$ the moments reach a maximum which may not be exceeded during any shock period.

The Eulerian buckling load ($a_E = 1$) thus represents

a remarkable boundary for the case of shock load. But, while denoting a stability limit for the static case, beyond which the bar fails,* it may be safely exceeded in dynamic load provided the period of loading is short enough and the crushing limit of the material is not exceeded thereby. To illustrate: If in our particular case the shock period is 0.6 times the period of the free fundamental oscillation of the bar ($b = 0.6$), the maximum stress upon exceeding the Euler load by about 17 percent ($a_E = 1.167$) is only about as high as the highest possible stress under a shock load, which is about 14 percent ($a_E = 0.864$) below the Euler load whereby, however, the latter is reached only with a longer shock period ($b = 1.2$).

To gain an insight into the order of magnitudes of the shock periods τ (equivalent to the range of b values in this report) and the allowable maximum "relative original eccentricities" $\left(5.86 \frac{\epsilon_o}{l}\right)$** several examples have been computed in table V.

From (75) and (54) follows:

$$\tau = \frac{2\pi b}{\chi_{o1}^2}\sqrt{\frac{\rho F}{EJ}} = \frac{32}{25\pi}\, l\, \frac{l}{i}\, b\sqrt{\frac{\rho}{E}} \qquad (104)$$

Besides, since our investigation applies only to conditions in which the stresses must remain below the proportionality limit, it follows that

$$\frac{M_{max}}{W} + \frac{P}{F} \leqq \sigma_p$$

which may also be expressed as

$$\frac{\epsilon_o}{l}\,\frac{EJ}{W}\,\frac{l^2}{\epsilon_o}\left|\frac{\partial^2 \eta}{\partial x^2}\right|_{max} \leqq \sigma_p - \frac{P}{F}$$

and the highest permissible "relative original eccentricity" is:

---

*The approximate differential equation of the problem is based upon these arguments. (See VII,1.)

**See equation (48).

$$5.86\,\frac{\epsilon_o}{l} \leqq 5.86\,\frac{lW}{EJ}\,\frac{\sigma_p - \frac{P}{F}}{\frac{l^2}{\epsilon_o}\left|\frac{\partial^2\eta}{\partial x^2}\right|_{max}} \qquad (105)$$

The $\frac{l^2}{\epsilon_o}\left|\frac{\partial^2\eta}{\partial x^2}\right|_{max}$ values are given in figure 19.

Table V gives (104) and (105) for a normal steel tube of 48/1 mm diameter with a proportionality limit of σ_p = 2,250 kg/cm^2, for a high-tensile 24/1 mm diameter steel tube with σ_p = 4,200 kg/cm^2 proportionality limit and a 48/1 mm diameter duralumin tube with σ_p = 1,400 kg/cm^2, each for a load stage 23 percent below and 16.7 percent above the Eulerian load.* Two bar lengths were considered for the lower stage; the shortest corresponds to the minimum slenderness

$$\frac{l}{i} = 4.5\sqrt{\frac{E}{\sigma_p}},$$

to which the Eulerian load is yet applicable (compare (98)), the longest one to $\frac{l}{i}$ = 200. At the upper stage only $\frac{l}{i}$ = 200 was considered, since the concept: boundary slenderness conformal to Euler, is without meaning.

It is seen that the permissible eccentricities decrease as the shock periods and loads increase. A criterion for the evaluation of the computed eccentricities is Müller-Breslau's recommended $\frac{1}{200}$ = 0.005.

The order of magnitude of the shock periods in the analyzed examples is 0.001 to 0.07 second.

In reality it should be possible to exceed the eccentricities of (105) without danger, for the elongation and elasticity limit decisive for the dynamic loads is probably higher than the corresponding limits for static loads (reference 8). The execution of systematic studies for the determination of the limit of dynamic elongation and

*The σ_p and E values are taken from A. Rechtlich's report, published in the 1931 DVL Yearbook, p. 379; and Schröder's report as published in the 1928 DVL Yearbook, p. 216.

elasticity of materials used in bridge and airplane design should be well worth while.

Likewise it is very desirable to check the results of this study by actual test. The writer hopes to be able to do this in the near future.

3. Range of Validity of the Approximate Differential Equation

A check on whether and to what extent the use of the equation in which $\left(\frac{\partial \eta}{\partial x}\right)^2$ was disregardod, is admissible. To this end we attempt to determine whether the $\left(\frac{\partial \eta}{\partial x}\right)^2$ values are actually small against 1. (See IV,5.)

The check may be confined to the maximum deflections after the actual shock, since, as shown in VII,2, they are nearly always greater than those during the shock.

Equation (59) gives:

$$\frac{\partial \eta}{\partial x} = \sum_n A_n \lambda_{on} \sin (p_{on} \bar{t} + \varphi) (\operatorname{sh} \lambda_{on} x + \sin \lambda_{on} x - \operatorname{ch} \lambda_{on} x + \cos \lambda_{on} x) \qquad (106)$$

The individual place functions in this sum are maximum or minimum for

$$\frac{d^2 \eta_x}{dx^2} = \lambda_{on}^2 (\operatorname{ch} \lambda_{on} x + \cos \lambda_{on} x - \operatorname{sh} \lambda_{on} x - \sin \lambda_{on} x) = 0$$

or

$$e^{\lambda_o x} = \sin \lambda_o x - \cos \lambda_o x \qquad (107)$$

when omitting the indices n and considering

$$\operatorname{ch} \lambda_o x - \operatorname{sh} \lambda_o x = e^{-\lambda_o x}$$

Equation (107) is resolved with

$$\lambda_o x = 1.036,\ 3.91,\ \sim \frac{9}{4}\pi,\ \sim \frac{13}{4}\pi,\ \sim \frac{17}{4}\pi$$

For the fundamental oscillation $\lambda_o l = \frac{5}{4}\pi$ is appli-

cable. Consequently, $\frac{\partial \eta}{\partial x}$ becomes maximum either for

$$\frac{x}{l} = \frac{4 \times 1.036}{5\,\pi} = 0.263$$

or

$$\frac{x}{l} = \frac{4 \times 3.91}{5\,\pi} = 0.995$$

The evaluation gives:

$$\frac{d\eta_x}{d\,x} = 1.019 \quad \text{for} \quad \frac{x}{l} = 0.263$$

$$\frac{d\eta_x}{d\,x} = -\,1.434 \quad \text{for} \quad \frac{x}{l} = 0.995$$

Hence $\frac{x}{l} = 0.995$ is decisive for the fundamental oscillation. We substitute here $\frac{x}{l} = 1.00$ for which, likewise, $\frac{d\eta_x}{d\,x}$ = approximately - 1.434 is valid.

But for $\frac{x}{l} = 1.00$, the place functions of all higher oscillations also reach a maximum or minimum, since the higher solutions of (107) agree with the higher proper values of our differential equation. Specifically, it is

$$\max \left|\frac{d\eta_{xn}}{dx}\right| \cong \sin \frac{4n+1}{4}\,\pi + \cos \frac{4n+1}{4}\,\pi = 2 \sin \frac{\pi}{4} = 1.414$$

since

$$e^{-\lambda_o x} = \operatorname{ch} \lambda_o x - \operatorname{sh} \lambda_o x$$

becomes negligibly small for higher values of $\lambda_o x$.

By the same arguments as used in VI,3,a, we obtain as upper limit value for $\max |\partial\eta/\partial x|$:

$$\left|\frac{\partial \eta}{\partial x}\right| = 1.434\, A_1\, \lambda_{o1} - 1.414 \sum_{n=2}^{\infty} A_n\, \lambda_{on} \qquad (108)$$

Now $\left|\frac{\partial \eta}{\partial x}\right| \frac{l}{\epsilon_o}$ can be computed from (108) by means of tables I and III, which contain the $\frac{A_n}{\epsilon_o}$ values. For $\frac{\epsilon_o}{l}$ the permissible eccentricities (see VII,2) must be included.

This calculation was carried through for the examples of table V and compiled in table VI.

Limiting the eccentricity $\frac{\epsilon_o}{l}$ so as to keep the stresses during the shock below the proportionality limit, the $\left|\frac{\partial \eta}{\partial x}\right|$ values for a stated bar and stated shock load scarcely depend on the shock period; furthermore, the $\left|\frac{\partial \eta}{\partial x}\right|$ values above the Eulerian limit are even smaller than those below it.

In the examples the maximum is $\left(\frac{\partial \eta}{\partial x}\right)^2 = 0.082^2 = 0.007$ for a high-tensile steel tube (24 × 1 mm, $l = 163$ cm, $P_E = 750$ kg) at $a = 0.77$ and $b = 0.10$, that is, for a comparatively small shock load and shock period. Even this $\max \left(\frac{\partial \eta}{\partial x}\right)^2$ may be summarily disregarded against 1.

The use of the approximate differential equation is herewith proved as justified.

APPENDIX

Derivation of the interference functions for the second and third Euler case.

For the pin-ended support as shown in figure 21, we have: for $x \leqq \xi$ the differential equation of the elastic line, because of

$$M = \underline{A}\, x + P\, \eta = \frac{l - \xi}{l}\, x + P\, \eta$$

at

$$E\, J\, \frac{d^2\eta}{dx^2} + P\, \eta = - \frac{l - \xi}{l}\, x$$

which resolved, becomes:

$$\eta = A \sin \omega\, x + B \cos \omega\, x - \frac{l - \xi}{P\, l}\, x$$

where

$$\omega^2 = \frac{P}{EJ}.$$

The limit condition $\eta = 0$ for $x = 0$ gives $B = 0$. Consequently,

$$\eta = A \sin \omega x - \frac{l - \xi}{P l} x \qquad (109)$$

For $x \geq \xi$ the differential equation is:

$$E J \frac{d^2\eta}{dx^2} + P \eta = - \frac{l - \xi}{l} x + (x - \xi)$$

and its resolution is:

$$\eta = \bar{A} \sin \omega x + \bar{B} \cos \omega x - \frac{l - x}{P l} \xi$$

The limit condition $\eta = 0$ for $x = l$ gives:

$$\bar{B} = - \bar{A} \tan \omega l,$$

consequently,

$$\eta = \bar{A} (\sin \omega x - \tan \omega l \cos \omega x) - \frac{l - x}{P l} \xi \qquad (110)$$

The determination of constants A and $\bar{A}$ follows from the continuity conditions at $x = \xi$. For this point the η values of (109) and (110), as well as their first derivatives, must be mutually equal. Equating (109) and (110) for $x = \xi$ gives:

$$A = \bar{A} (1 - \tan \omega l \cot \omega \xi) \qquad (111)$$

Equating the first derivative gives:

$$A \cos \omega \xi - \bar{A} (\cos \omega \xi + \tan \omega l \sin \omega \xi) = \frac{1}{P \omega} \qquad (112)$$

Then (111) and (112) yield:

$$\bar{A} = - \frac{\sin \omega \xi}{P \omega \tan \omega l}$$

$$A = \frac{\sin \omega (l - \xi)}{P \omega \sin \omega l}$$

and (109) and (110) become:

$$K_l (x, \xi) = \frac{\sin \omega (l - \xi)}{P \omega \sin \omega l} \sin \omega x - \frac{l - \xi}{P l} x \text{ for } x \leq \xi$$

$$K_r (x, \xi) = \frac{\sin \omega (l - x)}{P \omega \sin \omega l} \sin \omega \xi - \frac{l - x}{P l} \xi \text{ " } x \geq \xi$$

where we use η in place of $K(x,\xi)$. As seen, the core functions in x and ξ actually are symmetrical.

At the expense of much more paper work, although fundamentally with the same degree of accuracy as in the case of figure 21, the core functions may be obtained for other support conditions. For the bar clamped at one end and hinged at the other, for example (see fig. 22), the unknown support pressure $\underline{A}$ occurs in addition to the four constants A, B, A, and B. The conditions for resolving these five quantities are:

$$\eta_l = 0 \quad \text{for} \quad x = 0$$

$$\eta_r = 0 \quad " \quad x = l$$

$$\eta_l = \eta_r \quad " \quad x = \xi$$

$$\eta_r' = 0 \quad " \quad x = l$$

$$\eta_r' = \eta_l' \quad " \quad x = \xi$$

wherein subscripts l and r denote the parts of the elastic line on the left- and right-hand side of $x = \xi$. The calculation gives the following symmetrical core functions:

For $x \leq \xi$

$$K_l(x,\xi) = \frac{1}{P}\frac{\xi \sin \omega x + x \sin \omega\xi - \omega x\ \xi \cos \omega l - \frac{1}{\omega}\left[\sin\omega(\xi-l) + \omega l \cos \omega(\xi-l)\right]\sin \omega x}{\sin \omega l - \omega l \cos \omega l} - \frac{x}{P}$$

for $x \geq \xi$

$$K_r(x,\xi) = \frac{1}{P}\frac{x \sin \omega\xi + \xi \sin \omega x - \omega x\ \xi \cos \omega l - \frac{1}{\omega}\left[\sin\omega(x-l) + \omega l \cos \omega(x-l)\right]\sin \omega\xi}{\sin \omega l - \omega l \cos \omega l} - \frac{\xi}{P}$$

REFERENCES

1. Koning, Carel, and Taub, Josef: Impact Buckling of Thin Bars in the Elastic Range Hinged at Both Ends. T.M. No. 748, N.A.C.A., 1934.

2. Sezawa, Katsutade: Some Problems of Shocks Transmitted in Bars and in Plates. Aeronautical Research Institute Report No. 45, Tokyo Imperial University, 1928.

3. Love-Timpe: Lehrbuch der Elastizität (Teubner 1907), Sections 281-283. (See also bibliography, p. 32.)

4. Lamb, H. On Waves in an Elastic Plate. Proc. Roy. Soc., vol. 93, 1917.

   Geiger-Scheel: Hdb. d. Physik, vol. VI, p. 324.

5. Trefftz: Zur Frage der Holmfestigkeit. Z.F.M., vol. IX, nos. 15/16, 1918, pp. 101-103.

6. Hort: Die Differentialgleichungen des Ingenieurs. Springer, 1925, p. 657.

7. Courant-Hilbert: Methoden der mathematischen Physik, I. Springer, 1924, pp. 245 and 284.

8. Körber-v. Storp: Über den Kraftverlauf bei der Schlagprüfung. Mitt. d. K.W.G. f. Eisenforschung 56. Abhandlung.

TABLE I. Coefficients A_n of Series (59) for $a < 1$

a	b	$\frac{A_n}{\epsilon_o}$				$100\frac{A_n}{A_1}$		
		n=1	n=2	n=3	n=4	n=2	n=3	n=4
						percent		
0.25	0.10	0.159	-0.00052	-0.00008		0.33	0.05	
	0.30	0.453	-0.00282	-0.00054		0.62	0.12	
	0.556	0.632	-0.00488	-0.00095		0.77	0.15	
0.50	0.10	0.349	-0.00263	-0.00036		0.75	0.10	
	0.25	0.896	-0.0113	-0.00188		1.26	0.21	
	0.50	1.694	-0.0291	-0.00505		1.72	0.30	
	0.651	1.863	-0.0332	-0.00572		1.78	0.31	
0.75	0.10	0.571	-0.00746	-0.00096	-0.00025	1.31	0.17	0.04
	0.30	1.962	-0.04595	-0.00724	-0.00199	2.34	0.37	0.10
	0.50	3.595	-0.1028	-0.01658	-0.00460	2.86	0.46	0.13
	0.859	5.232	-0.1622	-0.02636	-0.00733	3.11	0.50	0.14
0.84	0.10	0.680	-0.0103	-0.00132	-0.00028	1.51	0.19	0.04
	0.25	1.928	-0.0470	-0.00725	-0.00193	2.44	0.38	0.10
	0.50	4.755	-0.1533	-0.0246	-0.00690	3.22	0.52	0.15
	0.75	7.565	-0.266	-0.0431	-0.0120	3.48	0.57	0.16
	1.040	8.972	-0.322	-0.0520	-0.0146	3.58	0.58	0.16
0.91	0.10	0.771	-0.0137	-0.00167	-0.00042	1.78	0.22	0.05
	0.25	2.245	-0.064	-0.00939	-0.00247	2.84	0.42	0.11
	0.50	5.94	-0.222	-0.0340	-0.00902	3.74	0.57	0.15
	0.75	10.50	-0.426	-0.0657	-0.01745	4.06	0.63	0.17
	1.00	14.58	-0.610	-0.0940	-0.02500	4.18	0.64	0.17
	1.34	16.90	-0.716	-0.1106	-0.02940	4.24	0.65	0.17
0.95	0.10	0.819	-0.0159	-0.00189	-0.00047	1.94	0.23	0.06
	0.25	2.425	-0.0748	-0.01062	-0.00280	3.08	0.44	0.12
	0.50	6.695	-0.2695	-0.0399	-0.01060	4.02	0.60	0.15
	0.75	12.64	-0.5515	-0.0823	-0.02195	4.36	0.65	0.17
	1.00	19.22	-0.867	-0.1296	-0.0345	4.51	0.67	0.18
	1.50	29.43	-1.355	-0.2027	-0.0541	4.60	0.69	0.18
	1.764	31.03	-1.432	-0.2144	-0.0572	4.61	0.69	0.19
0.99	0.10	0.877	-0.0185	-0.0022	-0.00043	2.11	0.25	0.05
	0.50	7.67	-0.3333	-0.0485	-0.0105	4.34	0.63	0.14
	1.00	26.00	-1.257	-0.185	-0.0403	4.84	0.71	0.16
	1.50	53.05	-2.622	-0.388	-0.0845	4.95	0.73	0.16
	2.00	84.50	-4.21	-0.623	-0.1358	4.98	0.74	0.16
	2.50	115.20	-5.76	-0.852	-0.1858	5.00	0.74	0.16
	3.00	139.9	-7.01	-1.038	-0.2260	5.02	0.74	0.16
	3.50	154.9	-7.76	-1.149	-0.2510	5.02	0.74	0.16
	3.845	158.0	-7.93	-1.173	-0.2560	5.02	0.74	0.16

TABLE II. Phase Displacements φ_n of Series (59) for $a < 1$

a	b	φ_n			
		n=1	n=2	n=3	n=4
0.25	0.10	0.3131	0.810	1.144	
	0.30	0.8988	1.330	1.454	
	0.556	$\pi/2$	$\pi/2$	$\pi/2$	
0.50	0.10	0.3097	0.783	1.122	
	0.25	0.7242	1.224	1.398	
	0.50	1.2588	1.468	1.521	
	0.651	$\pi/2$	$\pi/2$	$\pi/2$	
0.75	0.10	0.3074	0.799	1.134	1.304
	0.30	9.8969	1.176	1.430	1.489
	0.50	1.1489	1.433	1.504	1.532
	0.859	$\pi/2$	$\pi/2$	$\pi/2$	$\pi/2$
0.84	0.10	0.3127	0.809	1.410	1.309
	0.25	0.7004	1.220	1.414	1.469
	0.50	1.1111	1.419	1.505	1.528
	0.75	1.3638	1.505	1.543	1.553
	1.038	$\pi/2$	$\pi/2$	$\pi/2$	$\pi/2$
0.91	0.1	0.3589	0.796	1.131	1.303
	0.25	0.6820	1.208	1.391	1.465
	0.50	1.0597	1.400	1.488	1.522
	0.75	1.2716	1.476	1.525	1.544
	1.00	1.4153	1.523	1.598	1.557
	1.34	$\pi/2$	$\pi/2$	$\pi/2$	$\pi/2$
0.95	0.10	0.3043	0.794	1.131	1.302
	0.25	0.6729	1.202	1.388	1.463
	0.50	1.0339	1.389	1.483	1.519
	0.75	1.2255	1.447	1.518	1.540
	1.00	1.3448	1.500	1.536	1.551
	1.50	1.5030	1.550	1.561	1.565
	1.764	$\pi/2$	$\pi/2$	$\pi/2$	$\pi/2$
0.99	0.10	0.3020	0.790	1.112	1.300
	0.50	1.0100	1.379	1.474	1.516
	1.00	1.2787	1.478	1.525	1.595
	1.50	1.3878	1.514	1.542	1.555
	2.00	1.4493	1.533	1.552	1.560
	2.50	1.4910	1.546	1.558	1.564
	3.00	1.5290	1.554	1.563	1.566
	3.50	1.552	1.565	1.568	1.569
	3.845	$\pi/2$	$\pi/2$	$\pi/2$	$\pi/2$

TABLE III. Coefficients A_n of Series (59) for $a > 1$

a	b	$\frac{A_n}{\epsilon_o}$				$100\,\frac{A_n}{A_1}$		
		n=1	n=2	n=3	n=4	n=2	n=3	n=4
						percent		
1.01	0.10	0.911	-0.0201	-0.00230	-0.00028	2.21	0.25	0.03
	0.25	2.768	-0.0969	-0.01338	-0.00173	3.50	0.48	0.06
	0.50	8.20	-0.371	-0.0532	-0.0070	4.52	0.65	0.09
	0.75	17.22	-0.843	-0.1219	-0.016	4.76	0.71	0.09
	1.00	30.4	-1.530	-0.2220	-0.029	5.03	0.73	0.10
	1.50	71.5	-3.688	-0.536	-0.070	5.16	0.75	0.10
	2.00	138.7	-7.21	-1.048	-0.137	5.20	0.76	0.10
1.05	0.10	0.974	-0.0238	-0.0026	-0.00064	2.44	0.27	0.07
	0.25	3.025	-0.1163	-0.0155	-0.00393	3.85	0.51	0.13
	0.50	9.44	-0.466	-0.0645	-0.01652	4.94	0.68	0.18
	0.75	21.47	-1.140	-0.1593	-0.0408	5.31	0.74	0.19
	1.00	41.9	-2.285	-0.3205	-0.0823	5.46	0.77	0.20
1.09	0.10	1.072	-0.0293	-0.00314	-0.00075	2.73	0.29	0.07
	0.25	3.414	-0.1448	-0.01858	-0.0047	4.24	0.54	0.14
	0.50	11.36	-0.617	-0.0818	-0.0209	5.44	0.72	0.18
	0.75	28.20	-1.629	-0.2195	-0.0561	5.78	0.78	0.20
	1.00	61.70	-3.660	-0.4930	-0.1262	5.93	0.80	0.20

TABLE IV. Phase Displacements φ_n of Series (59) for $a > 1$

a	b	φ_n			
		n=1	n=2	n=3	n=4
1.01	0.10	0.3010	0.788	1.126	1.307
	0.25	0.6630	1.349	1.427	1.464
	0.50	0.9949	1.452	1.476	1.516
	0.75	1.1573	1.490	1.506	1.534
	1.00	1.2457	1.509	1.521	1.542
	1.50	1.3360	1.527	1.536	1.551
	2.00	1.3788	1.535	1.542	1.554
1.05	0.10	0.3024	0.802	1.127	1.300
	0.25	0.6571	1.198	1.381	1.459
	0.50	0.9703	1.367	1.470	1.511
	0.75	1.1117	1.423	1.498	1.528
	1.00	1.1823	1.448	1.510	1.535
1.09	0.10	0.3024	0.786	1.130	1.300
	0.25	0.6473	1.184	1.378	1.457
	0.50	0.9413	1.350	1.464	1.508
	0.75	1.0630	1.401	1.489	1.523
	1.00	1.1164	1.422	1.499	1.528

TABLE V. Illustrative Examples of Highest Permissible Relative Original Eccentricities y_{max}/l for Different Tubes Under Different Shock Loads P and Different Shock Periods τ.

Steel tube 48/1 mm $\begin{cases} E = 2\times10^6 \text{ kg/cm}^2 \\ \sigma_P = 2250 \text{ "} \end{cases}$

a_E	b	P_E=3330 kg $\begin{cases} \frac{l}{i} = 134 \\ l = 223 \text{ cm} \end{cases}$			P_E=1500 kg $\begin{cases} \frac{l}{i} = 200 \\ l = 332 \text{ cm} \end{cases}$		
		P	τ	$\frac{y_{max}}{l}$	P	τ	$\frac{y_{max}}{l}$
		kg	s		kg	s	
0.770	0.10	2560	0.0024	0.0126	1160	0.0054	0.0533
	0.25		0.0061	0.0042		0.0136	0.0179
	0.50		0.0122	0.0016		0.0271	0.0070
	0.75		0.0183	0.0010		0.0406	0.0043
	1.04		0.0254	0.0009		0.0564	0.0037
1.167	0.10				1755	0.0054	0.0234
	0.25					0.0136	0.0069
	0.50					0.0271	0.0020
	0.75					0.0406	0.0008
	1.00					0.0542	0.0003

(mm × .03937 = in.) (cm × .3937 = in.)

(kg × 2.20462 = lb.) (kg/cm^2 × 14.2235 = lb./sq.in.)

TABLE V (continued)

Steel tube 24/1 mm $\begin{cases} E = 2\times10^6 \text{ kg/cm}^2 \\ \sigma_p = 4200 \text{ "} \end{cases}$

a_E	b	P_E=3050 kg $\begin{cases} \frac{l}{i} = 98 \\ l = 80 \text{ cm} \end{cases}$			P_E=750 kg $\begin{cases} \frac{l}{i} = 200 \\ l = 163 \text{ cm} \end{cases}$		
		P	τ	$\frac{y_{max}}{l}$	P	τ	$\frac{y_{max}}{l}$
		kg	s		kg	s	
0.770	0.10	2345	0.0006	0.0167	565	0.0027	0.1214
	0.25		0.0016	0.0056		0.0067	0.0409
	0.50		0.0032	0.0022		0.0133	0.0160
	0.75		0.0048	0.0014		0.0200	0.0100
	1.04		0.0067	0.0011		0.0277	0.0084
1.167	0.10				855	0.0027	0.0649
	0.25					0.0067	0.0191
	0.50					0.0133	0.0055
	0.75					0.0200	0.0022
	1.00					0.0266	0.0010

Duralumin tube 48/1 mm $\begin{cases} E = 0.75\times10^6 \text{ kg/cm}^2 \\ \sigma_p = 1400 \text{ "} \end{cases}$

a_E	b	P_E=2060 kg $\begin{cases} \frac{l}{i} = 104 \\ l = 173 \text{ cm} \end{cases}$			P_E=560 kg $\begin{cases} \frac{l}{i} = 200 \\ l = 332 \text{ cm} \end{cases}$		
		P	τ	$\frac{y_{max}}{l}$	P	τ	$\frac{y_{max}}{l}$
		kg	s		kg	s	
0.770	0.10	1585	0.0014	0.0165	435	0.0053	0.1068
	0.25		0.0036	0.0056		0.0132	0.0360
	0.50		0.0072	0.0022		0.0264	0.0141
	0.75		0.0108	0.0014		0.0396	0.0087
	1.04		0.0149	0.0011		0.0549	0.0074
1.167	0.10				655	0.0053	0.0561
	0.25					0.0132	0.0165
	0.50					0.0264	0.0047
	0.75					0.0396	0.0019
	1.00					0.0530	0.0009

TABLE VI. Upper Limit Values of $\left|\frac{\partial \eta}{\partial x}\right|$ for the Examples of Table V

a	a_E	b	Upper limit of $\lvert\partial\eta/\partial x\rvert$ for: Steel tube diameter 48×1 mm P_E=1500 kg l = 332 cm $\frac{l}{i}$ = 200	Steel tube diameter 24×1 mm P_E=750 kg l =163 cm $\frac{l}{i}$ =200	Duralumin tube diameter 48×1 mm P_E = 560 kg l = 332 cm $\frac{l}{i}$ = 200
			Eccentricity $\frac{y_{max}}{l}$ according to table V		
0.84	0.770	0.10	0.036	0.082	0.072
		0.25	0.034	0.080	0.070
		0.50	0.034	0.079	0.069
		0.75	0.034	0.079	0.068
		1.04	0.034	0.075	0.068
1.09	1.167	0.10	0.026	0.070	0.061
		0.25	0.025	0.069	0.059
		0.50	0.024	0.067	0.058
		0.75	0.024	0.067	0.058
		1.00	0.020	0.067	0.058

Translation by J. Vanier,
National Advisory Committee
for Aeronautics.

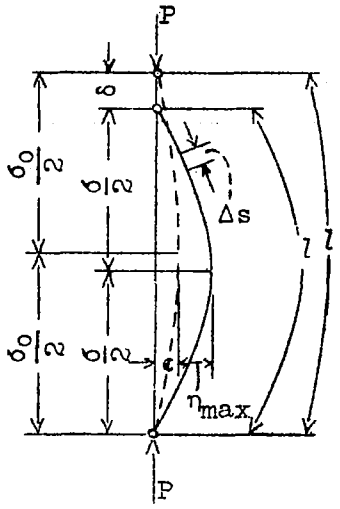

Figure 1a.- The bar hinged at both ends under tension P.

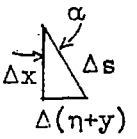

Figure 1b.- Element of bar of figure 1a.

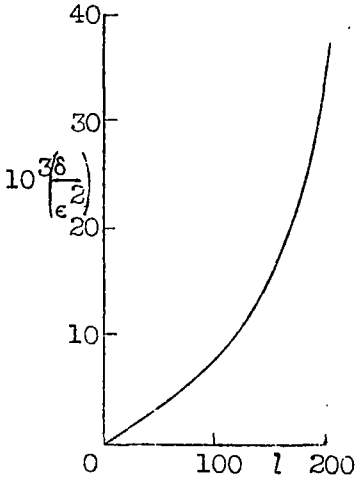

Figure 2. $\frac{\delta}{\epsilon^2 l}$ (see fig.1a) versus length of bar.

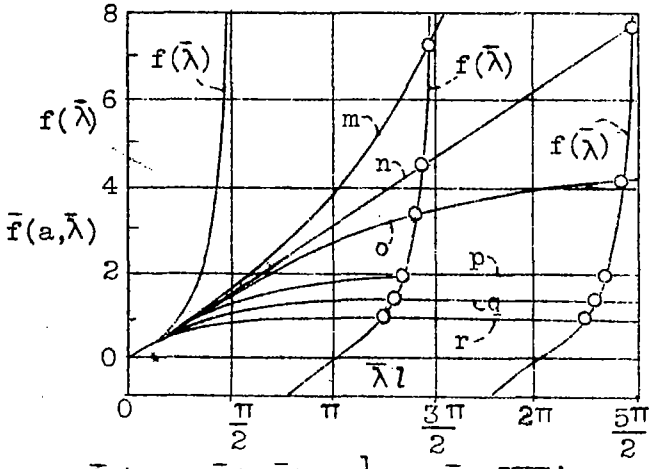

m, $\bar{f}$ for a =1.05
n, $\bar{f}$ for a =1.00 (Eulerian load)
o, $\bar{f}$ for a =0.95
p, $\bar{f}$ for a =0.75
q, $\bar{f}$ for a =0.5
r, $\bar{f}$ for a =0.0

Figure 3.-Determination of proper values for type of support corresponding to 3rd Eulerian case as abscissa of curves $f(\bar{\lambda}) = \tan \bar{\lambda} l$ and $\bar{f}(a,\bar{\lambda}) = \frac{1}{\sqrt{1-a}} \operatorname{th}(\bar{\lambda} l \sqrt{1-a})$. (parameter a).

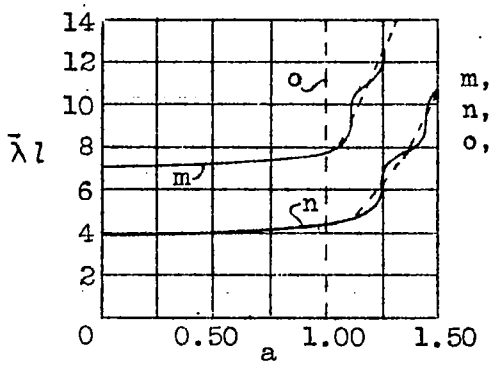

m, 1.Upper oscillation
n, Fundemental "
o, Eulerian load

Figure 4.-$\bar{\lambda} l$ for the fundemental oscillation and first upper oscillation of a bar conformably to Euler case, plotted against a .

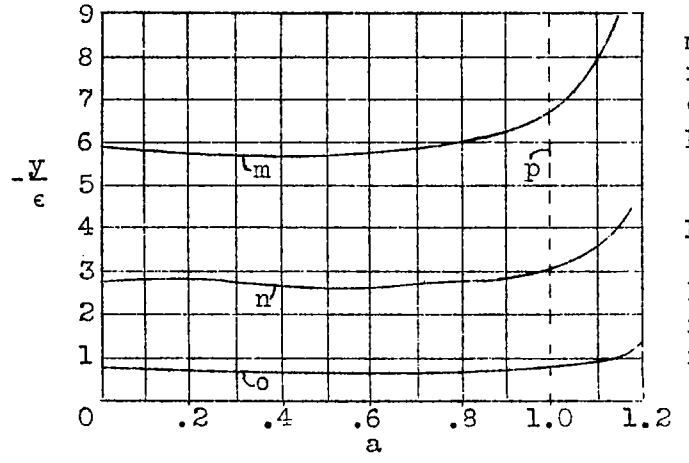

m, $x = l$
n, $x = 3/4\ l$
o, $x = 1/2\ l$
p, Eulerian load
(point of discontinuity)

Figure 5.-Deviations of bar form from straight line according to (46) for $x = l$, $x = 3/4\ l$, and $x = 1/2\ l$ versus a.

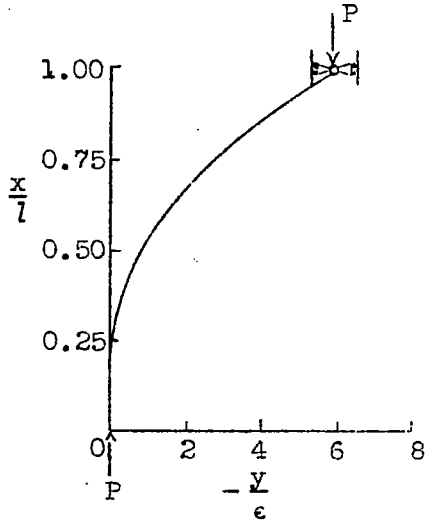

Figure 6.-The original bar form $\frac{y}{\epsilon}$ for a = 0.

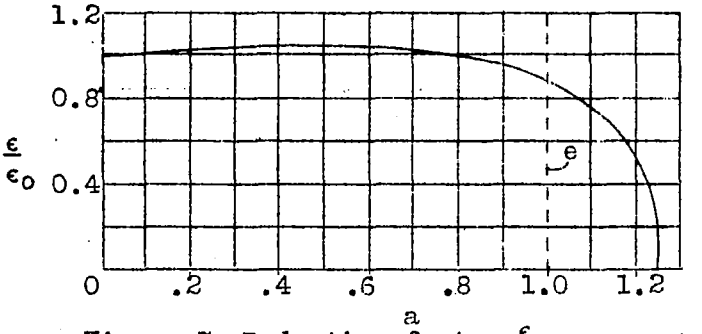

e, Eulerian load (point of discontinuity)

Figure 7.-Reduction factor $\frac{\epsilon}{\epsilon_o}$ versus a.

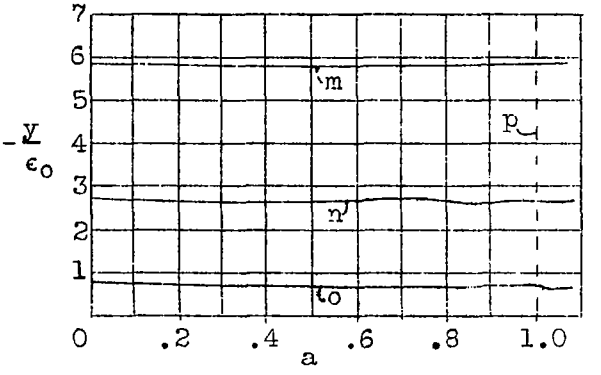

m, $x = l$
n, $x = 3/4\ l$
o, $x = 1/2\ l$
p, Eulerian load (point of discontinuity)

Figure 8.-Deviations of bar from straight line (according to (49) for $x = l$, $x = 3/4\ l$, and $x = 1/2\ l$ versus a.

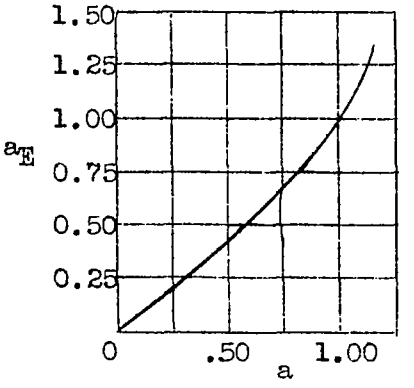

Figure 9.-Equation (52).

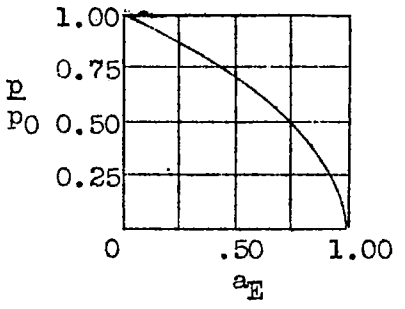

Figure 10.-Ratio of fundemental frequency for $a_E P_E$ and $\frac{p}{p_0}$ versus a_E.

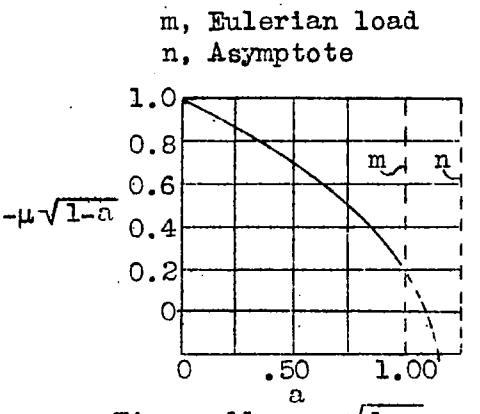

Figure 11.- $-\mu\sqrt{1-a}$ versus a.

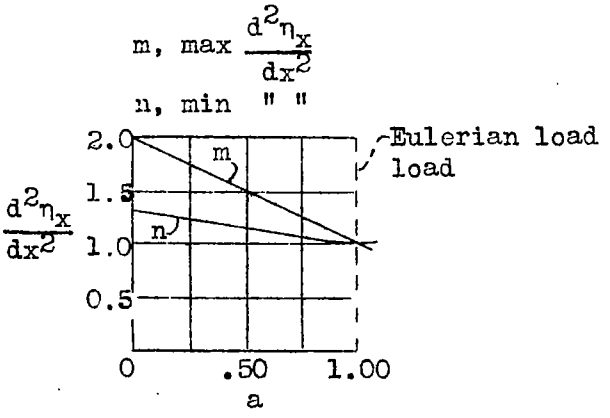

Figure 12.-Maximum and minimum (absolute) of $\frac{d^2\eta_x}{dx^2}$ versus a.

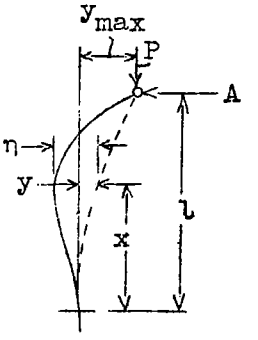

Figure 13.-Elastic line of a bar supported according to 3rd Eulerian load case and under force P with a given eccentricity.

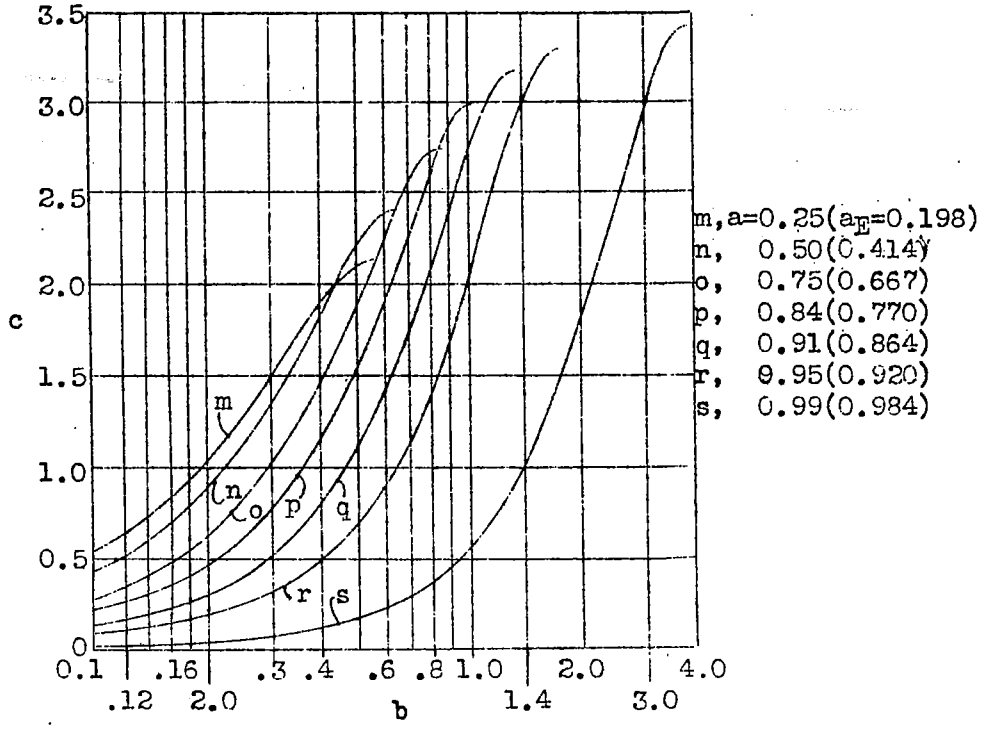

Figure 14.-Ratio c of absolute assumed maximum moments in static and dynamic case for support according to 3rd Eulerian case versus b proportional to shock period.(Parameter a_E denotes ratio of shock force to Eulerian buckling force).

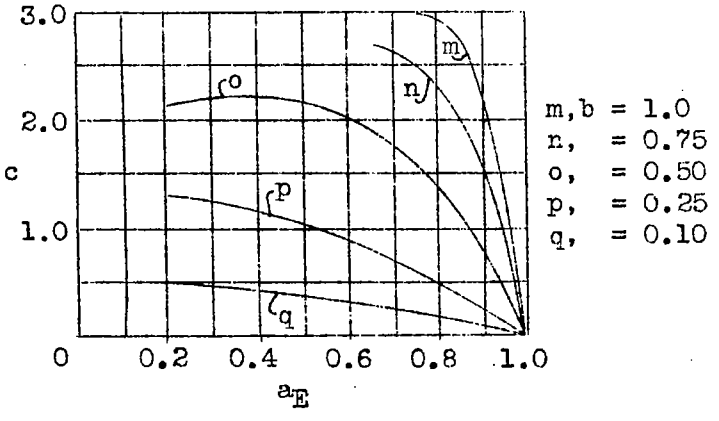

Figure 15.-Replotting of fig.14 (c versus a_E,parameter b).

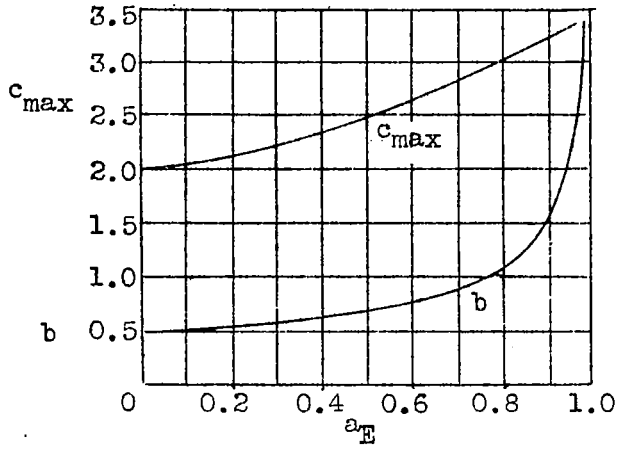

Figure 16.-Maximum possible c(for constant shock force and support according to 3rd Euler case)and c values(shock period)versus a_E.

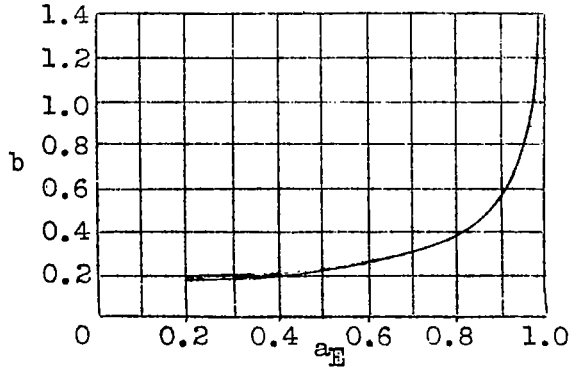

Figure 17.-Shock period (b) for different (a_E) at which static and dynamic stress are equal.

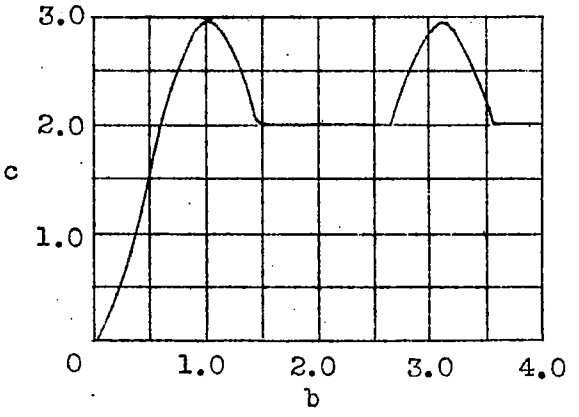

Figure 18.-Ratio c for a_E = 0.77 and a greater range of shock period (b).

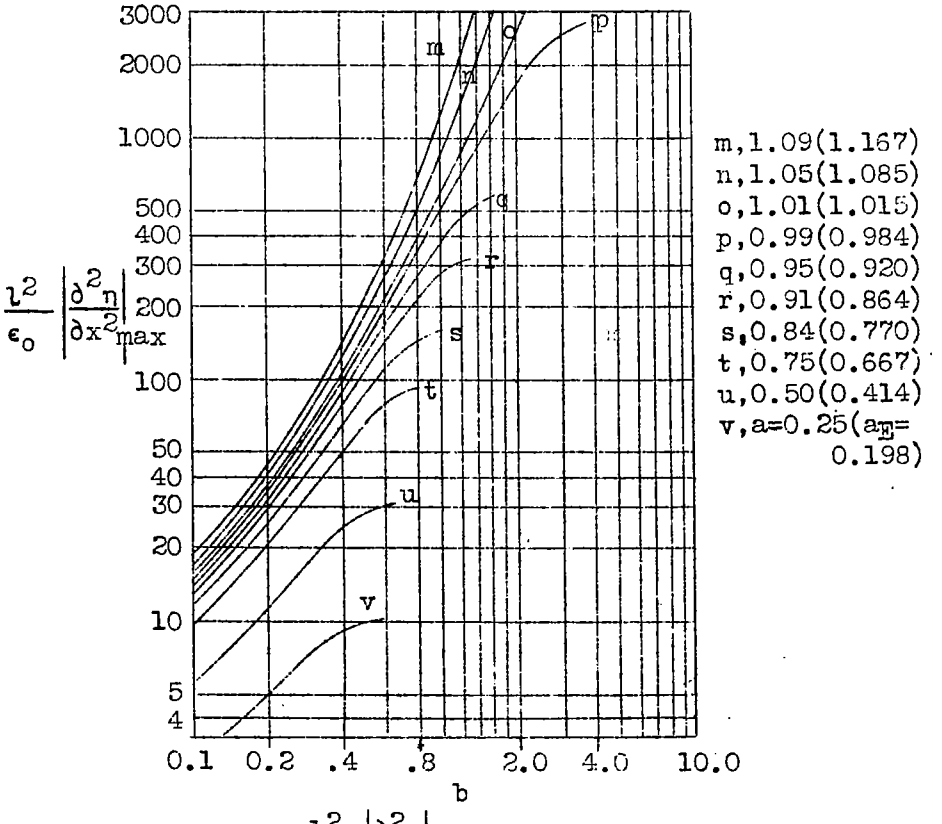

Figure 19.- $\frac{l^2}{\epsilon_o}\left|\frac{\partial^2\eta}{\partial x^2}\right|_{max}$ versus b.

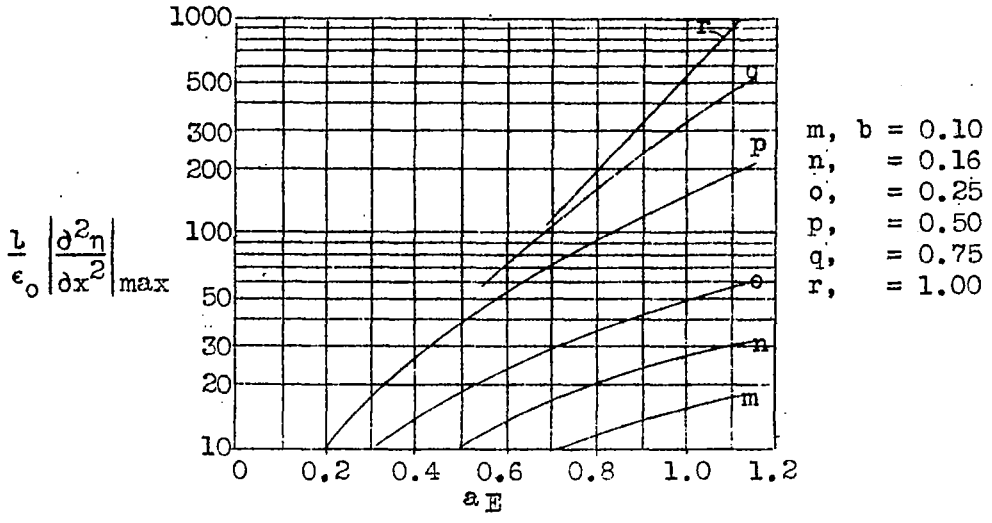

Figure 20.-$\frac{l^2}{\epsilon_0}\left|\frac{\partial^2\eta}{\partial x^2}\right|_{max}$ versus a_E, parameter b.

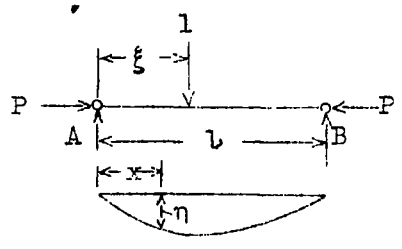

Figure 21.-Elastic line of bar hinged at either end and stressed in compression P and single transverse load l.

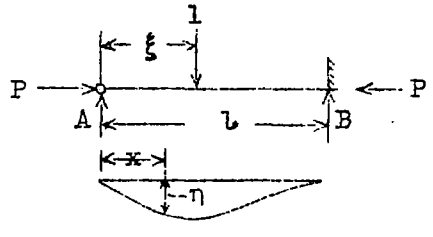

Figure 22.-Elastic line of bar clamped at one and hinged at the other end under load P and a single transverse load l.